RIPK1 Suppresses a TRAF2-Dependent Pathway to Liver Cancer

Anne T Schneider, Jérémie Gautheron, Maria Feoktistova, Christoph Roderburg, Sven H Loosen, Sanchari Roy, Fabian Benz, Peter Schemmer, Markus W Büchler, Ueli Nachbur, et al.

RIPK1 suppresses a TRAF2-dependent pathway to liver cancer

Anne T. Schneider[1,2,12], Jérémie Gautheron[1,2,12], Maria Feoktistova[3], Christoph Roderburg[1], Sven H. Loosen[1], Sanchari Roy[1], Fabian Benz[1], Peter Schemmer[8], Markus W. Büchler[8], Ueli Nachbur[9], Ulf P. Neumann[4], Rene Tolba[5], Mark Luedde[10], Jessica Zucman-Rossi[11], Diana Panayotova-Dimitrova[3], Martin Leverkus[3]†, Christian Preisinger[6], Frank Tacke[1], Christian Trautwein[1], Thomas Longerich[7], Mihael Vucur[1,2,*] and Tom Luedde[1,2,13,*]

[1] Department of Medicine III

[2] Division of Gastroenterology, Hepatology and Hepatobiliary Oncology

[3] Department of Dermatology and Allergology

[4] Department of Visceral and Transplantation Surgery

[5] Department of Laboratory Animal Research

[6] Proteomics Facility, IZKF

[7] Department of Pathology

RWTH Aachen University, D-52074 Aachen, Germany

[8] Department of Visceral and Transplantation Surgery, University of Heidelberg, D-69120 Heidelberg, Germany

[9] Walter and Eliza Hall Institute of Medical Research and Department of Medical Biology, University of Melbourne, Victoria 3050/3052, Australia

[10] Department of Cardiology, University Hospital, D-24105 Kiel, Germany

[11] INSERM, UMR-1162, Functional Genomic of Solid Tumors, Paris, France

[12] Co-first author

[13] Lead Contact

† This paper is dedicated to the memory of Prof. Dr. Martin Leverkus

* Correspondence: mvucur@ukaachen.de (M.V.), tluedde@ukaachen.de (T.Lu.)

SUMMARY

Receptor-interacting-protein-kinase-1 (RIPK1) represents an essential signaling-node in cell death and inflammation. Ablation of *Ripk1* in liver parenchymal cells (LPC) did not cause a spontaneous phenotype, but led to TNF-dependent hepatocyte apoptosis and liver injury without affecting inducible NF-κB activation. Loss of *Ripk1* induced the TNF-dependent proteasomal degradation of the E3-ligase TRAF2 in a kinase-independent manner, thereby activating Caspase-8. Moreover, loss of both *Ripk1* and *Traf2* in LPC not only resulted in Caspase-8 hyper-activation but also impaired NF-κB activation, promoting the spontaneous development of hepatocellular carcinoma (HCC). In line, low RIPK1 and TRAF2 expression in human HCCs was associated with an unfavorable prognosis, suggesting that RIPK1 collaborates with TRAF2 to inhibit murine and human hepatocarcinogenesis.

Keywords

SIGNIFICANCE

Cell death is an essential driver for the progression of chronic liver diseases towards HCC, suggesting that targeting of cell-death mediators might be an etiology-independent option for chemoprevention of liver cancer. RIPK1 is known to mediate programmed cell death and was suggested to promote cancer in specific genetic contexts, but the implication for human hepatocarcinogenesis has remained unclear. Here, we show that RIPK1 withholds a kinase-activity independent pro-survival-function in liver cells. Moreover, our data in mice and HCC-patients suggest that the TRAF2-dependent anti-carcinogenic function of RIPK1 might be of exceptional relevance in murine and human hepatocarcinogenesis. A better understanding of the pleiotropic pathways controlled by RIPK1 might open the road to additional strategies against HCC without unwanted off-target toxicities.

INTRODUCTION

Cell death represents a fundamental driver of liver disease progression and the development of liver fibrosis, cirrhosis and hepatocellular carcinoma (HCC) (Luedde et al., 2014; Vucur et al., 2010). Apoptotic death of hepatocytes is a common feature of viral hepatitis, acute liver failure, alcoholic and non-alcoholic steatohepatitis (Luedde et al., 2014) and is associated with fibrosis (Feldstein and Gores, 2005). However, a growing number of recent studies showed that there are distinct programmed cell death modes other than apoptosis. As such, necroptosis – relying on receptor-interacting-protein-kinase-3 (RIPK3) – represents an additional form of programmed cell death in development, tissue homeostasis and inflammation (Linkermann and Green, 2014). In the liver, necroptosis is involved in the mediation of non-alcoholic steatohepatitis (Gautheron et al., 2014) and was shown to counterbalance apoptosis in *Tak1*-deficient hepatocytes (Bettermann et al., 2010; Vucur et al., 2013), WT hepatocytes and adipocytes (Gautheron et al., 2016), but its general role in murine and human hepatocarcinogenesis is presently not well understood.

The kinase RIPK1 exerts strategic control over multiple pathways involved in regulating inflammation and cell death, and its diverse functions are controlled by posttranscriptional modification steps including phosphorylation and ubiquitination (Ofengeim and Yuan, 2013). Next to promoting necroptosis by assembling with RIPK3 (Linkermann and Green, 2014), in vitro-studies suggested that RIPK1 can promote the assembly of a RIPK1-dependent apoptosis complex, which proceeds through a RIPK1–FADD (Fas-associated-death-domain-protein) scaffold to activate Caspase-8 (Wilson et al., 2009). Beyond the activation of cell death pathways, it was suggested that RIPK1 is needed for activation of NF-κB (Kelliher et al., 1998), but this hypothesis was challenged by other studies (Wong et al., 2010).

It was recently shown in mice with conditional deletion of the IκB-Kinase (IKK) subunit *Nemo* that RIPK1's kinase activity contributes to the mediation of cell death and liver cancer (Kondylis et al., 2015). However, it was also demonstrated in a clinically relevant injury model of acetaminophen-toxicity that cell-death is mediated independently of RIPK1 in hepatocytes

(Schneider et al., 2015), suggesting that RIPK1 might play a different role in NEMO-competent liver cells, prompting us to study the hepatic function of RIPK1.

RESULTS

Normal Liver Development and Homeostasis in Mice with Conditional Deletion of *Ripk1* in Parenchymal Liver Cells

Mice with constitutive deletion of *Ripk1* in all body cells appear normal at birth but fail to thrive and die at 1-3 days of age (Kelliher et al., 1998). Therefore, to examine the hepatic function of RIPK1 in liver homeostasis and liver injury, we generated a genetically modified mouse line with exons 4 and 5 of the *Ripk1* gene flanked by loxP sites (RIPK1^{FL}) (Figure 1A). RIPK1^{FL} mice were then interbred with alfp-Cre mice (Kellendonk et al., 2000) to generate animals with conditional deletion of *Ripk1* in liver parenchymal cells (LPC) (RIPK1^{LPC-KO}) (Figure 1A).

RIPK1^{LPC-KO} mice were born at normal Mendelian ratio and appeared macroscopically normal at birth and at 6 weeks of age. Efficient deletion of *Ripk1* in LPC of 6-week-old RIPK1^{LPC-KO} mice was demonstrated on DNA level by PCR from tail-extracts and on protein level by Western blot analysis on whole liver extracts and extracts from primary hepatocytes (Figure 1B and 1C). Serological analyses in 6-week-old and 50-week-old mice did not reveal alterations in aspartate aminotransferase (AST), alanine aminotransferase (ALT) and glutamate dehydrogenase (GLDH) levels between RIPK1^{LPC-KO} and wild-type (WT) control mice (Figure 1D), indicating absence of spontaneous liver cell death. In line, the liver architecture of 6-week-old RIPK1^{LPC-KO} mice was not significantly altered as shown by H/E staining (Figure 1E). Additional quantification of immune cells revealed normal numbers of F4/80$^+$ monocytes/macrophages, CD3$^+$ T-cells and B220$^+$ B-cells in RIPK1^{LPC-KO} livers compared to WT controls (Figure S1A). The amount of proliferating hepatocytes was also not altered in RIPK1^{LPC-KO} mice (Figure S1B). Finally, RIPK1^{LPC-KO} mice did not show any increased lethality over WT controls until the age of 50 weeks and displayed no histological alterations at that age (Figure 1E). Together, these data suggest that RIPK1 is not essential to maintain liver homeostasis and cellular integrity of hepatocytes under physiological conditions.

Of note, it was previously shown that RIPK1-full-knockout mice (RIPK1$^{-/-}$) displayed large necrotic regions in the liver and cleaved (cl.) Caspase-3$^+$ liver cells (Rickard et al., 2014). We therefore compared livers from our conditional knockouts with RIPK1$^{-/-}$ mice sacrificed around birth and confirmed liver damage and apoptosis in RIPK1$^{-/-}$ mice, which was absent in age-matched RIPK1^{LPC-KO} livers (Figures S1C and S1D). The most likely explanation for this striking difference is the fact that RIPK1$^{-/-}$ mice show increased cell death in multiple organs including their intestine (Rickard et al., 2014), presumably leading to the release of inflammatory factors that reach the liver via the portal vein where they might induce cell-death of *Ripk1*-deficient hepatocytes.

Ablation of *Ripk1* Promotes Acute LPS/TNF-Mediated Hepatocyte Apoptosis and Liver Injury in an NF-κB and JNK-Independent Manner

Based on these previous findings, we wanted to examine if *Ripk1*-deficient liver cells might be susceptible to death-receptor induced cell death. We therefore injected 6-week-old RIPK1^{LPC-KO} mice and WT controls with bacterial lipopolysaccharide (LPS), which indirectly induces hepatocellular death through stimulation of tumor necrosis factor (TNF) secretion from hepatic immune cells. In line with previous results (Luedde et al., 2008), injection of LPS in a dose of 2.5 µg/g bodyweight did not lead to elevation of serum AST, ALT or GLDH levels in WT mice (Figure 2A). In contrast, RIPK1^{LPC-KO} mice displayed a massive increase in these parameters, suggesting acute hepatic damage 8 hr after LPS injection (Figure 2A). On histological level, RIPK1^{LPC-KO} livers revealed inflammatory foci with focally detectable cl. Caspase-3$^+$ hepatocytes (Figure 2B), suggesting that apoptosis was involved in the mediation of liver injury in these mice. In line, Western blot analysis revealed increased cleavage of Caspase-8 and the executioner Caspase-3 peaking at 4 hr after LPS-injection in *Ripk1*-deficient livers (Figure 2C), confirming activation of LPS/TNF-dependent apoptosis upon *Ripk1*-deletion. Together, these findings provide evidence that loss of *Ripk1* enforces LPS-induced liver injury and hepatocellular apoptosis, underlining the functional difference

between its survival function in hepatocytes and the pro-apoptotic role demonstrated in many other experimental systems (Dickens et al., 2012).

Low or medium doses of TNF do normally not trigger apoptosis in liver cells unless activation of NF-κB is inhibited or transcription of NF-κB-dependent anti-apoptotic factors is blocked (Luedde and Schwabe, 2011). Given the putative role of RIPK1 in NF-κB activation (Kelliher et al., 1998), we hypothesized that increased sensitivity of RIPK1[LPC-KO] livers to LPS might be related to defective activation of NF-κB. However, in line with previous findings (Wong et al., 2010), Western blot analysis on whole liver extracts from LPS-stimulated mice revealed no differences in the degradation of IκBα – the inhibitor of NF-κB (Luedde and Schwabe, 2011) – between RIPK1[LPC-KO] and WT livers (Figure 2C). To exclude a possible overlap with the regulation of NF-κB in *Ripk1*-proficient immune cells in livers of RIPK1[LPC-KO] mice, we isolated primary hepatocytes from WT and RIPK1[LPC-KO] livers, stimulated them with TNF, and performed Electro-Mobility-Shift-Assay (EMSA) and qRT-PCR analysis for the NF-κB target genes *A20* and *IκBα*. These experiments confirmed full activation of NF-κB upon TNF stimulation in *Ripk1*-deficient hepatocytes (Figures 2D and 2E), showing that TNF-dependent NF-κB activation is not depending on the presence of RIPK1 in hepatocytes.

Finally, we analyzed how *Ripk1*-deletion affected activation of Jun-(N)-terminal Kinase (JNK), a kinase associated with the regulation of hepatocyte apoptosis (Luedde et al., 2014). RIPK1[LPC-KO] livers showed increased JNK activation at 4 hr after LPS injection that correlated with maximum Caspase-activation in these livers (Figure 2C), suggesting that JNK might be involved in the apoptosis pathway activated in the absence of *Ripk1*. To test this, we treated LPS-injected RIPK1[LPC-KO] mice with the JNK-inhibitor SP600125 (Gautheron et al., 2014; Vucur et al., 2013) or vehicle (DMSO). Treatment with SP600125 resulted in an efficient blockage of the phosphorylation of the JNK substrate c-Jun compared with vehicle treated mice at 8 hr after LPS treatment (Figure S2A). However, SP600125-treatment did not result in a significant change in liver enzymes between both groups 8 hr after LPS injection (Figure S2B). In line, the number of cl. Caspase-3[+] hepatocytes as well as the amount of cl. Caspase-3 on Western blot analysis was not significantly different between DMSO- and

SP600125-treated mice (Figures S2A, S2C and S2D). These data provide evidence that JNK activation was not a necessary step for Caspase-8 activation and apoptosis in *Ripk1*-deficient hepatocytes and suggested that JNK was rather activated in response to apoptosis, probably mediating secondary effects like compensatory regeneration (Vucur et al., 2013).

Ripk1 Ablation Promotes LPS/TNF-Dependent Activation of Caspase-8 in Hepatocytes in a RIPK3-dependent Manner

We next wanted to genetically test if LPS/TNF-dependent cell-death in the absence of RIPK1 was only mediated by activation of Caspase-8, or if RIPK3-dependent necroptosis might be involved in this process. To test this, we generated mice with combined ablation of *Ripk1* and *Caspase-8* in LPC (RIPK1/Casp-8^{LPC-KO}) as well as mice with combined conditional deletion of *Ripk1* in LPC and constitutive ablation of *Ripk3* in all body cells (RIPK1^{LPC-KO}/RIPK3$^{-/-}$) (Figure S3A) and compared their phenotypes upon LPS stimulation with WT and *Ripk1*-single mutant mice. Additional deletion of *Caspase-8* completely rescued RIPK1^{LPC-KO} mice from liver injury and hepatocyte apoptosis, as demonstrated by serological analysis (Figure 3A) and expression of cl. Caspase-3 and TUNEL assay (Figures 3B-3E), suggesting that absence of RIPK1 triggers the activation of Caspase-8 and subsequently of Caspase-3 in hepatocytes upon LPS stimulation. In contrast, additional ablation of *Ripk3* did not prevent elevation of liver injury markers in the absence of *Ripk1* at 8 hr after LPS stimulation (Figure 3A), suggesting that necroptosis does not significantly contribute to liver injury in this context. However, a more detailed examination at different time points revealed that the peak of Caspase-3 cleavage was significantly delayed in RIPK1^{LPC-KO}/RIPK3$^{-/-}$ mice compared to RIPK1^{LPC-KO} mice (Figures 3B-3E).

These findings were validated by Western blotting (Figures 3F and 3G). Of note, JNK activation peaked at 4 hr after LPS-injection in RIPK1^{LPC-KO} mice and after 8 hr in RIPK1^{LPC-KO}/RIPK3$^{-/-}$ mice, closely following the activation of Caspase-8 and Caspase-3, suggesting that JNK was activated in response to Caspase activation in these respective mouse livers (Figures 3F and 3G). Finally, neither additional ablation of *Caspase-8* nor *Ripk3* changed the

competence of *Ripk1*-deficient livers to activate NF-κB as shown by Western blot for the degradation of IκBα (Figures 3F and 3G) and confirmed by EMSA analysis in livers and hepatocytes stimulated with LPS or TNF respectively (Figures S3B and S3C). Together, these findings indicate that RIPK1 mediates a survival signal in the context of LPS-mediated liver injury by preventing direct, NF-κB-independent activation of Caspase-8. Moreover, absence of RIPK1 in hepatocytes switches the function of RIPK3 from a pure mediator of necroptosis to a promoter of early hepatocyte apoptosis after LPS stimulation.

Loss of a Kinase-Independent Scaffolding Function of RIPK1 Leads to Proteasomal Degradation of TRAF2 in Hepatocytes

We aimed at further defining the mechanism how Caspase-8 activation and cell death were mediated in response to LPS stimulation in *Ripk1*-deficient hepatocytes. It has been suggested that RIPK1 can influence the expression levels of the TNF Receptor Associated Factor (TRAF) family member TRAF2 – a ubiquitin ligase involved in NF-κB activation – in mouse embryonic fibroblast (MEF) cells (Gentle et al., 2011). Importantly, recent studies suggested that TRAF2 has an anti-apoptotic function in cells and that ablation of *Traf2* can trigger apoptosis by an NF-κB-independent mechanism (Gonzalvez et al., 2012; Karl et al., 2014). Moreover, RIPK1 and TRAF2 have been found in a large inducible protein complex (Lamkanfi et al., 2005) and it was suggested that TRAF2 can bind RIPK1 directly via its N-terminus (Takeuchi et al., 1996). To test if a TNF-dependent complex of RIPK1 and TRAF2 is formed in liver cells, we first stimulated human hepatoma cells (HepG2) with Fc-tagged TNF, followed by precipitation of the Fc-tag via Agarose G beads. As shown in Figure 4A, TNF stimulation resulted in recruitment of endogenous polyubiquitinated RIPK1, TRAF2, cellular-inhibitor-of-apoptosis-protein-1 (cIAP-1) and TNFR1-associated-death-domain-protein (TRADD) to the TNF-Receptor-1 (TNFR1). An additional co-IP on murine hepatoma cell (Hepa1-6) extracts with overexpressed and tagged RIPK1- and TRAF2-proteins confirmed binding between RIPK1 and TRAF2, which was increased by overexpression of ubiquitin (Figure S4A).

9

Next, we wanted to analyze if loss of *Ripk1* can influence TRAF2 expression levels after LPS/TNF stimulation in hepatocytes. As demonstrated in Figure 4B, TRAF2 expression levels remained stable in non-stimulated RIPK1[LPC-KO] livers and WT controls. Strikingly, LPS stimulation resulted in rapid disappearance of TRAF2 in *Ripk1*-deficient but not in WT livers (Figure 4B, upper panel). In line with these in vivo-findings, there was a striking decrease of TRAF2 in the soluble fraction of TNF-treated primary hepatocyte extracts from RIPK1[LPC-KO] mice compared to WT hepatocytes within 15 min (Figure 4B, middle section). Following this reduction, the amount of TRAF2 remained at low level without further decrease until 90 min after TNF (Figure 4B, lower panel). Of note, reduction of TRAF2 expression in the absence of *Ripk1* in hepatocytes was also detected in LPS-stimulated livers from RIPK1[LPC-KO]/RIPK3^{-/-} and RIPK1/Casp-8[LPC-KO] mice (Figures S4B and S4C), arguing for a direct control of TRAF2 levels by RIPK1 rather than a secondary regulation through cell death activation. Moreover, stimulation of RIPK1[LPC-KO] hepatocytes with the alternative death ligands FasL/CD95L or TRAIL had no influence on TRAF2 levels (Figures 4C and S4D). In contrast to TRAF2, cIAP-1 was not differently regulated in all respective mouse groups after LPS stimulation (Figures S4B and S4C). Similarly, cIAP-1 regulation did not differ between WT and *Ripk1*-deficient primary hepatocytes stimulated with TNF (Figure S4E), suggesting that cIAP-1 levels in hepatocytes did not depend on RIPK1 presence.

We further analyzed the RIPK1-dependent regulation of TRAF2 in primary hepatocytes. TNF treatment resulted in increased TRAF2 levels in the insoluble fraction (containing K48-poly-ubiquitinated proteins targeted for proteasomal degradation) of *Ripk1*-deficient primary hepatocyte lysates already 2 min after stimulation (Figure 4B, middle and lower panels). Pretreatment of primary hepatocytes with the proteasomal inhibitors Bortezomib (Figure 4D) or MG312 (Figure S4F) resulted in the accumulation of TRAF2 in the insoluble fraction of lysates from RIPK1[LPC-KO] hepatocytes stimulated with TNF, indicating that in the absence of RIPK1, TRAF2 is targeted for increased ubiquitination and proteasomal degradation in response to TNF stimulation. The fact that even without TNF stimulation, 4 hr of pretreatment with both proteasomal inhibitors led to a slight shift from

soluble to insoluble fractions in WT and *Ripk1*-deficient hepatocytes (compare lanes 4 with 1 and 10 with 7 in Figures 4D and S4F) indicated that there is a basal turnover of TRAF2, which was also increased by RIPK1 deficiency (compare lanes 10 with lanes 4 in both blots).

We next wanted to assess if degradation of TRAF2 upon *Ripk1*-ablation and TNF treatment was functionally related to the kinase function of RIPK1 or an alternative scaffolding function. For this, we performed Western blot analysis on protein lysates from TNF-stimulated primary hepatocytes and compared TRAF2 protein levels between *Ripk1*-deficient and WT hepatocytes pretreated with the RIPK1-kinase inhibitors Necrostatin-1s (Nec1s) and Nec1 (Figures 4E and S4G) (Takahashi et al., 2012), for which TNF-treated L929 cells served as a positive control (Figures S4H and S4I). Interestingly, no degradation of TRAF2 in TNF- and Nec1s/Nec1-treated WT hepatocytes was observed compared to RIPK1^LPC-KO hepatocytes upon TNF treatment, while TRAF2 expression was unchanged between Nec1s/Nec1-treated and –non-treated *Ripk1*-deficient hepatocytes (Figures 4E and S4G). To further confirm this finding, we injected LPS into mice constitutively expressing a kinase-dead mutant of RIPK1 (RIPK1^KD) (Berger et al., 2014) (Figure S4J) and stimulated also primary hepatocytes from these respective mice with TNF. Strikingly, kinase-inactivation did not lead to TNF-dependent TRAF2 degradation (Figure 4F). Thus, degradation of TRAF2 in response to TNF stimulation in RIPK1^LPC-KO hepatocytes was mediated through loss of a kinase-independent scaffolding function of RIPK1.

Co-Deletion of *Ripk1* and *Traf2* Triggers Spontaneous Hepatocyte Apoptosis, Hepatitis and Dysplasia

We next wanted to functionally confirm that TRAF2 is involved in cell death mediation in *Ripk1*-deficient liver cells. To test this hypothesis, we generated LPC-specific conditional mice with combined ablation of *Traf2* and *Ripk1* (RIPK1/TRAF2^LPC-KO) (Figure 5A) and compared their spontaneous phenotypes with WT controls and *Traf2*-single mutant mice (TRAF2^LPC-KO) at the age of 6 weeks. Similar to the previous findings in RIPK1^LPC-KO mice (Figure 1), livers of TRAF2^LPC-KO mice did not show a macroscopic alteration at 6 weeks of

11

age (Figure 5B). Moreover, TRAF2^{LPC-KO} single mutant mice showed only a slight elevation of AST, ALT, GLDH and alkaline phosphatase (AP) serum levels and histology revealed a mild and focal ductular reaction (Figures 5C and 5D). Finally, EMSA analysis on primary $Traf2$-deficient hepatocytes revealed a hyper-activation of NF-κB upon TNF stimulation (Figure S5A), indicating that the presence of TRAF2 in hepatocytes is not essential for NF-κB activation.

In contrast to the findings in RIPK1^{LPC-KO} and TRAF2^{LPC-KO} single mutant mice, combined ablation of $Ripk1$ and $Traf2$ in LPC resulted in the formation of macroscopically visible nodules and a cholestatic liver at 6 weeks of age (Figure 5B), associated with strong elevation of AST, ALT, GLDH and AP serum levels (Figure 5C). Histologically, RIPK1/TRAF2^{LPC-KO} mice showed a more severe hepatitis associated with inflammation compared to WT and TRAF2^{LPC-KO} mice (Figures S5B and S5C) as well as formation of dysplastic foci (Figure 5D). These data – together with the fact that RIPK1^{LPC-KO} did not show a spontaneous phenotype – suggest that RIPK1 and TRAF2 collaborate in LPC to prevent spontaneous development of liver injury, hepatitis and liver cell dysplasia.

We next tested if hepatitis and dysplasia development were associated with a dysregulation of apoptotic cell death and compensatory proliferation of LPC in RIPK1/TRAF2^{LPC-KO} mice. Strikingly, RIPK1/TRAF2^{LPC-KO} mice showed a significant increase in cl. Caspase-3$^+$ liver cells compared to WT and TRAF2^{LPC-KO} livers (Figure 5E), correlating with spontaneous cleavage of Caspase-8 and Caspase-3 on Western blot analysis (Figure 5F). Of note, spontaneous apoptosis was associated with strong compensatory proliferation of hepatocytes in RIPK1/TRAF2^{LPC-KO} livers, since approximately 30% of hepatocytes in these livers stained positive for Ki67 (Figure 5E), which went along with upregulation of CyclinD1 and PCNA in these livers on Western blot analysis (Figure 5F). Collectively, while single $Ripk1$-mutant mice were sensitive to TNF-induced apoptosis but did not display spontaneous cell death, our data in RIPK1/TRAF2^{LPC-KO} mice showed that the combined loss of $Ripk1$ and $Traf2$ in LPC triggers a sequence of spontaneous hepatocyte apoptosis, hepatic

inflammation and compensatory LPC proliferation, associated with the development of dysplastic foci in the liver.

Finally, we further analyzed how increased apoptosis was mediated in *Ripk1-* and *Traf2*-deficient hepatocytes. As shown in Figure 5F, spontaneous apoptosis in RIPK1/TRAF2^{LPC-KO} livers was associated with decreased levels of the anti-apoptotic proteins cFLIP$_L$ and cIAP-1. In line with reduced c-FLIP$_L$-levels, combined ablation of *Ripk1* and *Traf2* resulted in impaired NF-κB activation in LPS-stimulated livers and TNF-stimulated primary hepatocytes as demonstrated by nuclear staining for RelA/p65 (Figures 5G and 5H), EMSA (Figure 5I) and qRT-PCR for the NF-κB target genes *A20* and *IκBα* (Figure 5J). Collectively, these data suggest that in hepatocytes, RIPK1 and TRAF2 have a redundant function in the activation of NF-κB.

Hepatocarcinogenesis in RIPK1/TRAF2^{LPC-KO} Mice Depends on Caspase-8 Activation

We next wanted to test if the observed activation of hepatocyte apoptosis, inflammation and compensatory proliferation in the livers of mice with combined ablation of *Ripk1* and *Traf2* might influence hepatocarcinogenesis. To test this, we analyzed the phenotype of 50-52-week-old WT, RIPK1^{LPC-KO}, TRAF2^{LPC-KO} and RIPK1/TRAF2^{LPC-KO} mice. In line with the previous results at the age of 6 weeks, 50-week-old RIPK1^{LPC-KO} and 52-week-old TRAF2^{LPC-KO} mice did not show a macroscopic alteration and no change in their liver-weight / body-weight ratio compared to WT controls at the same age (Figures 6A and 6B). In contrast, 52-week-old RIPK1/TRAF2^{LPC-KO} mice displayed multiple large liver tumors and a strong increase in their liver-weight / body-weight ratio (Figures 6A and 6B). H/E and Collagen IV stainings and histopathological assessment revealed that these macroscopic tumors represented moderately to poorly differentiated hepatocellular carcinoma (HCC), that were present in every RIPK1/TRAF2^{LPC-KO} liver (Figures 6C, S6A and Table S1). HCC displayed a higher rate of apoptotic and proliferating cells compared with the non-tumorous surrounding, as shown by stainings for cl. Caspase-3 and Ki67 (Figure S6B). Therefore,

RIPK1 and TRAF2 in LPC collaborate to prevent the spontaneous development of liver cancer in mice.

Based on the pleiotropic pathways involved in carcinogenesis that might potentially be influenced by RIPK1 and TRAF2 (Luedde et al., 2014), we next wanted to functionally examine if activation of Caspase-8 was the primary reason for carcinogenesis in RIPK1/TRAF2^{LPC-KO} mice, or if other downstream targets of RIPK1 and/or TRAF2 mediated HCC development in these mice. To test this, we generated triple knockout mice deficient for *Ripk1*, *Traf2* and *Caspase-8* in LPC (RIPK1/TRAF2/Casp-8^{LPC-KO} mice) (Figure S6C) and examined their spontaneous phenotypes at the age of 6 and 52 weeks. Strikingly, RIPK1/TRAF2/Casp-8^{LPC-KO} mice showed a complete rescue from spontaneous liver injury at the age of 6 weeks, demonstrated by AST, ALT and GLDH values (Figure 6D), and a macroscopic and histological normalization at the same age (Figures 6E and 6F). Interestingly, additional ablation of *Caspase-8* fully restored cIAP-1 expression in RIPK1/TRAF2^{LPC-KO} mice (Figure 6G), suggesting that cIAP-1 down-regulation in RIPK1/TRAF2^{LPC-KO} mice occurred as a response to Caspase-8 activation as suggested previously (Guicciardi et al., 2011). In contrast, expression of the anti-apoptotic c-FLIP$_L$ form was still significantly reduced in RIPK1/TRAF2/Casp-8^{LPC-KO} mice compared to WT mice (Figure 6G). Together, these findings provide evidence that inhibition of NF-κB contributed to apoptosis induction in RIPK1/TRAF2^{LPC-KO} mice, while down-regulation of cIAP-1 levels occurred as a secondary effect in response to Caspase activation. Furthermore, additional deletion of *Caspase-8* in RIPK1/TRAF2^{LPC-KO} mice completely prevented hepatocarcinogenesis at the age of 52 weeks (Figures 6E and 6F). In contrast, additional deletion of *Ripk3* in RIPK1/TRAF2^{LPC-KO} mice (RIPK1/TRAF2^{LPC-KO}/RIPK3$^{-/-}$) did not significantly influence their spontaneous phenotype (Figures S6D-S6J). Together, these findings provide functional proof that hepatocarcinogenesis in RIPK1/TRAF2^{LPC-KO} mice depends on Caspase-8 activation.

We finally wanted to provide further evidence that – in addition to the NF-κB-independent control of Caspase-8 by TRAF2 – the functional redundancy in NF-κB activation

between RIPK1 and TRAF2 also contributed to the prevention of spontaneous hepatocarcinogenesis in RIPK1[LPC-KO] and TRAF2[LPC-KO] single mutant mice. For this, we generated mice with combined ablation of *Traf2* and the catalytic IκB-Kinase (IKK) subunit *Ikkβ* in LPC (TRAF2/IKKβ[LPC-KO] mice) (Figure 7A) and examined their spontaneous phenotypes at the age of 6 and 52 weeks. As shown by EMSA, NF-κB activation was inhibited in TRAF2/IKKβ[LPC-KO] mice (Figure 7B). Macroscopically, livers of TRAF2/IKKβ[LPC-KO] mice did not display alterations at 6 weeks of age (Figure 7C), but serological analyses revealed elevated AST, ALT and GLDH levels (Figure 7D) at this age. Histological analysis of liver sections from these animals revealed a mild and focal ductular reaction (Figures 7E) with a significant increase of cl. Caspase-3^{+} liver cells and compensatory proliferation (Figures 7E) compared to WT livers, which was confirmed by Western blot analysis (Figure S7A). At the age of 52 weeks, all TRAF2/IKKβ[LPC-KO] mice developed macroscopically visible tumors, which microscopically corresponded to mainly dysplastic foci and few advanced HCC (Figures 7F, 7G, S7B and Table S1). These data highlight that the preserved ability for NF-κB activation prevents spontaneous tumorigenesis in TRAF2[LPC-KO] and RIPK1[LPC-KO] mice (Koppe et al., 2016). Moreover, the fact that more advanced HCC were detected in RIPK1/TRAF2[LPC-KO] compared to TRAF2/IKKβ[LPC-KO] mice at the same age (Table S1) supported our hypothesis that, beyond NF-κB activation, RIPK1 also controls an NF-κB-independent, apoptosis and cancer checkpoint via TRAF2 (Figure 7H).

The Expression Status of RIPK1 and TRAF2 Influences Prognosis in Human HCC Patients

We finally aimed at providing evidence for a potential relevance of this respective anti-carcinogenic function of RIPK1 and TRAF2 in human liver cancer. For this, expression levels of RIPK1 and TRAF2 were assessed by tissue microarray analysis (TMA) in tumor tissues of 99 HCC patients with different etiologies of underlying liver disease undergoing liver resection (Geraud et al., 2013; Hoffmann et al., 2014) (Figure 8A and Table S2). As shown in Figures 8B and 8C, patients with low RIPK1 expression [immunoreactive (IR)-score <2]

displayed a trend for a worse prognosis. Moreover, patients with low TRAF2 expression in their tumors had a significantly worse prognosis compared to patients with higher TRAF2 expression (Figures 8D and 8E). Remarkably, combined higher expression of RIPK1 and TRAF2 in HCC was associated with a significant survival benefit, while HCC patients with low or undetectable expression of both RIPK1 and TRAF2 had the lowest probability for survival (Figures 8F and 8G). Together, these data indicate that RIPK1 and TRAF2 are variably expressed in human HCCs. In our retrospective analysis, low or absent expression of both molecules were associated with a worse outcome, providing evidence that our murine data on the role of RIPK1 and TRAF2 in HCC development might be of relevance for human hepatocarcinogenesis.

DISCUSSION

Here, we demonstrated that the kinase RIPK1 – that is associated with the promotion of both apoptosis and necroptosis in many cellular systems (Weinlich and Green, 2014) – represents a fundamental signaling node in LPC that inhibits a TRAF2- and Caspase-8-dependent apoptosis checkpoint and thereby controls liver cancer development. Of note, several previous studies suggested that the execution of cell death along these respective pathways represents the main function of RIPK1 in liver cells, thereby promoting liver injury and cancer. However, we showed that *Ripk1*-deficiency in hepatocytes did not influence APAP toxicity in mice (Schneider et al., 2015), suggesting that liver cell death in this model is mainly mediated through RIPK1-independent platforms. It was recently shown that in mice with deletion of *Nemo* in hepatocytes, a kinase-inactive mutant prevented hepatocyte apoptosis and HCC development (Kondylis et al., 2015). While to our knowledge no data exist that underpin a functional dependency of NEMO and RIPK1 in the initiation or progression of human HCC, it cannot be excluded that the apoptosis-promoting function of RIPK1's kinase activity might be of relevance in certain clinical settings of human liver injury. However, here we provide data that in NEMO-competent liver cells, RIPK1 primarily mediates an important survival signal via TRAF2 in the context of liver injury triggered by LPS and TNF.

Our findings together with previous data underline that kinase-dependent functions of RIPK1 need to be distinguished from kinase-independent "scaffolding"-functions, supporting the hypothesis that RIPK1 is a molecule with "two faces" (Weinlich and Green, 2014). We show that this respective scaffolding function of RIPK1 in hepatocytes prevents proteasomal degradation of TRAF2 in a kinase-independent manner. It is important to note that the RIPK1-dependent control of cell death and survival factors seems to be cell type specific. As such, in contrast to previous findings in gut or skin (Dannappel et al., 2014; Takahashi et al., 2014), conditional deletion of *Ripk1* in LPC did not cause spontaneous hepatocyte apoptosis and hepatitis. Moreover, *Caspase-8*-deficiency did not rescue the perinatal lethality of *Ripk1*-full-knockout mice, but prevented apoptosis in many tissues including intestine, thymus, liver

and lung (Dillon et al., 2014; Kaiser et al., 2014). One possible explanation for differences between liver and other organs might be that liver cells are confronted with microbial compounds like LPS more indirectly through the portal vein than gut or skin epithelial cells that are directly and permanently confronted with commensal bacteria. In addition, it was previously shown in mouse embryonic fibroblast (MEF) cells and tumor cells that cIAP-1 is degraded upon TNF stimulation in a RIPK1-dependent manner (Gentle et al., 2011; Vince et al., 2008), which in our experiments in hepatocytes was not the case.

It was also shown in lymphocytes from *Ripk1*-full-knockout mice that NF-κB activation in these cells was depending on the presence of RIPK1 (Kelliher et al., 1998). In contrast, along with previous findings (Wong et al., 2010), we show here that in hepatocytes, NF-κB can be activated in response to TNF independently of RIPK1. Interestingly, RIPK1/TRAF2[LPC-KO] mice showed impaired NF-κB activation in hepatocytes, suggesting that in *Ripk1*-deficient hepatocytes, even low levels of TRAF2 can replace the function of RIPK1 in NF-κB activation. Moreover, while defective NF-κB activation led to spontaneous apoptosis and carcinogenesis in RIPK1/TRAF2[LPC-KO] animals, our data highlight that TRAF2-degradation in RIPK1[LPC-KO] single mutant mice promoted apoptosis by an alternative, NF-κB-independent mechanism. Finally, our experiments in mice with combined deficiency of *Ripk1* and *Ripk3* revealed the interesting finding that in the absence of *Ripk1*, RIPK3 – the bona fide mediator of necroptosis – promotes a pro-apoptotic signal, based on the fact that RIPK1[LPC-KO]/RIPK3^{-/-} mice showed a significant delay in apoptosis upon LPS stimulation compared with RIPK1[LPC-KO] single mutants. While contradictory at first sight, RIPK3 is also found in the pro-apoptotic complex and might serve as a platform in this complex (Pasparakis and Vandenabeele, 2015).

Several previous studies suggested that targeting RIPK1 might be an interesting approach to combat inflammation in different organs (Bullock and Degterev, 2015). The role of this approach in cancer development has not been clear yet, but might be elucidated by comparison between mouse data and data from human cancer. As such, *RIPK1* is commonly up-regulated in human melanoma via DNA-copy-number gain and constitutive ubiquitination

(Liu et al., 2015) and a *RIPK1*-mutation was found in human HCC (Schulze et al., 2015). On a functional level, RIPK1 promoted tumor cell proliferation in an NF-κB-dependent manner (Liu et al., 2015) and additionally promoted survival of melanoma cells through activation of autophagy (Luan et al., 2015). Together, these data indicate that pharmacological targeting of the kinase-activity or pro-autophagic function of RIPK1 might be promising strategies in melanoma. Similarly, RIPK1 was suggested to promote breast cancer metastasis via NF-κB (Bist et al., 2011) and survival of pancreatic cancer cells against TRAIL-mediated apoptosis (Wang et al., 2007), providing further potential rationales for RIPK1-targeting in specific cancers. In contrast, our mouse data along with the fact that loss of RIPK1- and TRAF2 expression in human HCCs was associated with worse patients' prognoses provided evidence for an anti-carcinogenic role in the liver. The mechanisms underlying down-regulation of RIPK1 and TRAF2 expression in this respective subgroup of human HCCs and the relation to different steps along the sequence from dysplasia, tumor initiation and promotion of HCCs are currently not fully clear. It should be also noted that not all human HCCs that lost RIPK1 expression also showed down-regulation of TRAF2 and vice versa. Given that TRAF2 also suppresses activation of necroptosis (Petersen et al., 2015), we cannot exclude that TRAF2 and RIPK1 also control anti-tumorigenic pathways that are independent of each other, but our data strongly suggest that the RIPK1-TRAF2-Caspase-8 axis does influence the pathogenesis and prognosis of human HCC. Only if pro- and anti-carcinogenic functions of RIPK1 will be functionally understood and can be highly specifically targeted, this might be an option in a disease-specific context.

EXPERIMENTAL PROCEDURES

Generation of conditional knockout mice

A RIPK1 targeting vector containing exons 4 and 5 flanked with two loxP sites and an frt-flanked neomycin resistance gene cassette was obtained from KOMP Repository (CSD47184). JM8.N4 embryonic stem cells (ESCs) derived from C57BL/6N mice were transfected and selected as previously described (Pasparakis, 2005). Chimeric mice were generated by injection of ESCs into blastocysts from C57BL/6 mice. Matings of male chimeras to C57BL/6 female mice resulted in transmission of the floxed *Ripk1* allele to the germline. RIPK1$^{FL/FL-frt/frt}$ mice were bred with C57Bl/6 transgenic mouse line carrying the FlpO deleter (Kranz et al., 2010) to remove the neomycin resistance gene cassette. Finally, RIPK1$^{FL/FL}$ mice were crossed with alfp-Cre transgenic mice (Kellendonk et al., 2000) to generate a liver parenchymal cell (LPC)-specific knockout of *Ripk1* (RIPK1^{LPC-KO}).

Mice carrying LoxP-site-flanked (floxed) *Caspase-8* (Salmena et al., 2003) and *Traf2* alleles (Grech et al., 2004) were crossed to *alfp*-Cre transgenic mice (Kellendonk et al., 2000) to generate LPC-specific knockout mice. Mice with constitutive deletion of RIPK3 (RIP3$^{-/-}$), RIPK1-Kinase-dead (KD) mice, RIPK1-full-knockout mice (RIPK1$^{-/-}$) and IKKβ floxed mice were described before (Berger et al., 2014; Dillon et al., 2014; Maeda et al., 2003; Newton et al., 2004). In all experiments, littermates carrying the respective loxP-flanked alleles but lacking expression of Cre-recombinase were used as wild-type (WT) controls. Mice were bred on a mixed C57/BL6 - SV129Ola genetic background. Only sex- and age-matched animals were compared.

Liver injury models

Experiments were performed on 6-week-old male mice. LPS (Sigma-Aldrich) was administered i.p. at 2.5 mg/kg of body weight. Intraperitoneal injection of the JNK-Inhibitor SP600125 (1 mg, Absource Diagnostics) or vehicle Dimethyl Sulfoxide (DMSO, Sigma-Aldrich) was performed as described (Vucur et al., 2013). Male and female mice were used to analyze cancer development. All animal studies were approved by the Federal Ministry for

Nature, Environment and Consumers' Protection of the state of North Rhine-Westphalia and were ethically reviewed and carried out in accordance with European Directive 86/609/EEC and the GSK Policy on the Care, Welfare and Treatment of Animals.

Human Liver Samples

The human samples used in this study were approved by the local ethics committee of the University Hospital Heidelberg (approval no: 206/2005).

Quantification and statistical analysis

Mouse data were analyzed using PRISM software (GraphPad Software, Inc., La Jolla, CA) and are expressed as mean. Gaussian distribution was tested with Kolmogorov–Smirnov test. Differences between two groups were assessed by an unpaired two-sample t-test or Mann-Whitney test and multiple comparisons between more than two groups have been conducted by ANOVA with Bonferroni-test or Kruskal-Wallis test for post hoc analysis. Statistical analyses of human data were performed with SPSS Version 22 (SPSS, Chicago, IL, USA). Kaplan Meier curves were plotted to display the impact on survival and between-group differences were assessed using the log-rank test. All reported p values were two-tailed, and a p value less than 0.05 was considered indicating statistical significance.

SUPPLEMENTAL INFORMATION

Supplemental Information includes Supplemental Experimental Procedures, seven figures and two tables.

AUTHORS CONTRIBUTIONS

AT.S., J.G., M.V. and T.Lu. conceived and designed the experiments; AT.S. and J.G. performed and analyzed most of the experiments; C.R., C.P., J. Z-R., SH.L., S.R., F.B., U.N., M.F., and D.PD. contributed to the performance and analyses of experiments; M.L., R.T., UP.N., M.Le., C.T. and F.T. provided intellectual input; P.S., MW.B. and T. Lo. provided

human tumor samples and T.Lo. performed histopathological analyses; M.V. and T.Lu. supervised experiments; T.Lu., M.V., J.G. and AT.S. wrote the manuscript with help from other authors. M.V and T.Lu. contributed equally.

REFERENCES

Berger, S. B., Kasparcova, V., Hoffman, S., Swift, B., Dare, L., Schaeffer, M., Capriotti, C., Cook, M., Finger, J., Hughes-Earle, A., et al. (2014). Cutting Edge: RIP1 kinase activity is dispensable for normal development but is a key regulator of inflammation in SHARPIN-deficient mice. J Immunol *192*, 5476-5480.

Bettermann, K., Vucur, M., Haybaeck, J., Koppe, C., Janssen, J., Heymann, F., Weber, A., Weiskirchen, R., Liedtke, C., Gassler, N., et al. (2010). TAK1 suppresses a NEMO-dependent but NF-kappaB-independent pathway to liver cancer. Cancer Cell *17*, 481-496.

Bist, P., Leow, S. C., Phua, Q. H., Shu, S., Zhuang, Q., Loh, W. T., Nguyen, T. H., Zhou, J. B., Hooi, S. C., and Lim, L. H. (2011). Annexin-1 interacts with NEMO and RIP1 to constitutively activate IKK complex and NF-kappaB: implication in breast cancer metastasis. Oncogene *30*, 3174-3185.

Bullock, A. N., and Degterev, A. (2015). Targeting RIPK1,2,3 to combat inflammation. Oncotarget *6*, 34057-34058.

Dannappel, M., Vlantis, K., Kumari, S., Polykratis, A., Kim, C., Wachsmuth, L., Eftychi, C., Lin, J., Corona, T., Hermance, N., et al. (2014). RIPK1 maintains epithelial homeostasis by inhibiting apoptosis and necroptosis. Nature *513*, 90-94.

Dickens, L. S., Powley, I. R., Hughes, M. A., and MacFarlane, M. (2012). The 'complexities' of life and death: death receptor signalling platforms. Experimental Cell Research *318*, 1269-1277.

Dillon, C. P., Weinlich, R., Rodriguez, D. A., Cripps, J. G., Quarato, G., Gurung, P., Verbist, K. C., Brewer, T. L., Llambi, F., Gong, Y. N., et al. (2014). RIPK1 blocks early postnatal lethality mediated by caspase-8 and RIPK3. Cell *157*, 1189-1202.

Feldstein, A. E., and Gores, G. J. (2005). Apoptosis in alcoholic and nonalcoholic steatohepatitis. Frontiers In Bioscience : a journal and virtual library *10*, 3093-3099.

Gautheron, J., Vucur, M., Reisinger, F., Cardenas, D. V., Roderburg, C., Koppe, C., Kreggenwinkel, K., Schneider, A. T., Bartneck, M., Neumann, U. P., et al. (2014). A positive feedback loop between RIP3 and JNK controls non-alcoholic steatohepatitis. EMBO Molecular Medicine *6*, 1062-1074.

Gautheron, J., Vucur, M., Schneider, A. T., Severi, I., Roderburg, C., Roy, S., Bartneck, M., Schrammen, P., Diaz, M. B., Ehling, J., et al. (2016). The necroptosis-inducing kinase RIPK3 dampens adipose tissue inflammation and glucose intolerance. Nat Commun *7*, 11869.

Gentle, I. E., Wong, W. W., Evans, J. M., Bankovacki, A., Cook, W. D., Khan, N. R., Nachbur, U., Rickard, J., Anderton, H., Moulin, M., et al. (2011). In TNF-stimulated cells, RIPK1 promotes cell survival by stabilizing TRAF2 and cIAP1, which limits induction of non-canonical NF-kappaB and activation of caspase-8. The Journal of Biological Chemistry *286*, 13282-13291.

Geraud, C., Mogler, C., Runge, A., Evdokimov, K., Lu, S., Schledzewski, K., Arnold, B., Hammerling, G., Koch, P. S., Breuhahn, K., et al. (2013). Endothelial transdifferentiation in hepatocellular carcinoma: loss of Stabilin-2 expression in peri-tumourous liver correlates with increased survival. Liver Int *33*, 1428-1440.

Gonzalvez, F., Lawrence, D., Yang, B., Yee, S., Pitti, R., Marsters, S., Pham, V. C., Stephan, J. P., Lill, J., and Ashkenazi, A. (2012). TRAF2 Sets a threshold for extrinsic apoptosis by tagging caspase-8 with a ubiquitin shutoff timer. Molecular Cell *48*, 888-899.

Grech, A. P., Amesbury, M., Chan, T., Gardam, S., Basten, A., and Brink, R. (2004). TRAF2 differentially regulates the canonical and noncanonical pathways of NF-kappaB activation in mature B cells. Immunity *21*, 629-642.

Guicciardi, M. E., Mott, J. L., Bronk, S. F., Kurita, S., Fingas, C. D., and Gores, G. J. (2011). Cellular inhibitor of apoptosis 1 (cIAP-1) degradation by caspase 8 during TNF-related apoptosis-inducing ligand (TRAIL)-induced apoptosis. Experimental Cell Research *317*, 107-116.

Hoffmann, K., Muller-Butow, V., Franz, C., Hinz, U., Longerich, T., Buchler, M. W., and Schemmer, P. (2014). Factors predictive of survival after stapler hepatectomy of hepatocellular carcinoma: a multivariate, single-center analysis. Anticancer Res *34*, 767-776.

Kaiser, W. J., Daley-Bauer, L. P., Thapa, R. J., Mandal, P., Berger, S. B., Huang, C., Sundararajan, A., Guo, H., Roback, L., Speck, S. H., et al. (2014). RIP1 suppresses innate immune necrotic as well as apoptotic cell death during mammalian parturition. Proceedings of the National Academy of Sciences of the United States of America *111*, 7753-7758.

Karl, I., Jossberger-Werner, M., Schmidt, N., Horn, S., Goebeler, M., Leverkus, M., Wajant, H., and Giner, T. (2014). TRAF2 inhibits TRAIL- and CD95L-induced apoptosis and necroptosis. Cell Death & Disease *5*, e1444.

Kellendonk, C., Opherk, C., Anlag, K., Schutz, G., and Tronche, F. (2000). Hepatocyte-specific expression of Cre recombinase. Genesis *26*, 151-153.

Kelliher, M. A., Grimm, S., Ishida, Y., Kuo, F., Stanger, B. Z., and Leder, P. (1998). The death domain kinase RIP mediates the TNF-induced NF-kappaB signal. Immunity *8*, 297-303.

Kondylis, V., Polykratis, A., Ehlken, H., Ochoa-Callejero, L., Straub, B. K., Krishna-Subramanian, S., Van, T. M., Curth, H. M., Heise, N., Weih, F., et al. (2015). NEMO Prevents Steatohepatitis and Hepatocellular Carcinoma by Inhibiting RIPK1 Kinase Activity-Mediated Hepatocyte Apoptosis. Cancer Cell *28*, 582-598.

Koppe, C., Verheugd, P., Gautheron, J., Reisinger, F., Kreggenwinkel, K., Roderburg, C., Quagliata, L., Terracciano, L., Gassler, N., Tolba, R. H., et al. (2016). IkappaB kinasealpha/beta control biliary homeostasis and hepatocarcinogenesis in mice by phosphorylating the cell-death mediator receptor-interacting protein kinase 1. Hepatology *64*, 1217-1231.

Kranz, A., Fu, J., Duerschke, K., Weidlich, S., Naumann, R., Stewart, A. F., and Anastassiadis, K. (2010). An improved Flp deleter mouse in C57Bl/6 based on Flpo recombinase. Genesis *48*, 512-520.

Lamkanfi, M., D'Hondt, K., Vande Walle, L., van Gurp, M., Denecker, G., Demeulemeester, J., Kalai, M., Declercq, W., Saelens, X., and Vandenabeele, P. (2005). A novel caspase-2 complex containing TRAF2 and RIP1. The Journal of Biological Chemistry *280*, 6923-6932.

Linkermann, A., and Green, D. R. (2014). Necroptosis. The New England Journal of Medicine *370*, 455-465.

Liu, X. Y., Lai, F., Yan, X. G., Jiang, C. C., Guo, S. T., Wang, C. Y., Croft, A., Tseng, H. Y., Wilmott, J. S., Scolyer, R. A., et al. (2015). RIP1 Kinase Is an Oncogenic Driver in Melanoma. Cancer Res *75*, 1736-1748.

Luan, Q., Jin, L., Jiang, C. C., Tay, K. H., Lai, F., Liu, X. Y., Liu, Y. L., Guo, S. T., Li, C. Y., Yan, X. G., et al. (2015). RIPK1 regulates survival of human melanoma cells upon endoplasmic reticulum stress through autophagy. Autophagy *11*, 975-994.

Luedde, T., Heinrichsdorff, J., De Lorenzi, R., De Vos, R., Roskams, T., and Pasparakis, M. (2008). IKK1 and IKK2 cooperate to maintain bile duct integrity in the liver. Proc. Natl. Acad. Sci. USA *105*, 9733-9738.

Luedde, T., Kaplowitz, N., and Schwabe, R. F. (2014). Cell Death and Cell Death Responses in Liver Disease: Mechanisms and Clinical Relevance. Gastroenterology *147*, 765-783 e764.

Luedde, T., and Schwabe, R. F. (2011). NF-kappaB in the liver--linking injury, fibrosis and hepatocellular carcinoma. Nat Rev Gastroenterol Hepatol *8*, 108-118.

Maeda, S., Chang, L., Li, Z. W., Luo, J. L., Leffert, H., and Karin, M. (2003). IKKbeta is required for prevention of apoptosis mediated by cell-bound but not by circulating TNFalpha. Immunity *19*, 725-737.

Newton, K., Sun, X., and Dixit, V. M. (2004). Kinase RIP3 is dispensable for normal NF-kappa Bs, signaling by the B-cell and T-cell receptors, tumor necrosis factor receptor 1, and Toll-like receptors 2 and 4. Mol Cell Biol *24*, 1464-1469.

Ofengeim, D., and Yuan, J. (2013). Regulation of RIP1 kinase signalling at the crossroads of inflammation and cell death. Nature reviews Molecular Cell Biology *14*, 727-736.

Pasparakis, M. (2005). Making gene-modified mice. ErnstScheringResFoundWorkshop, 1-26.

Pasparakis, M., and Vandenabeele, P. (2015). Necroptosis and its role in inflammation. Nature *517*, 311-320.

Petersen, S. L., Chen, T. T., Lawrence, D. A., Marsters, S. A., Gonzalvez, F., and Ashkenazi, A. (2015). TRAF2 is a biologically important necroptosis suppressor. Cell Death and Differentiation *22*, 1846-1857.

Rickard, J. A., O'Donnell, J. A., Evans, J. M., Lalaoui, N., Poh, A. R., Rogers, T., Vince, J. E., Lawlor, K. E., Ninnis, R. L., Anderton, H., et al. (2014). RIPK1 regulates RIPK3-MLKL-driven systemic inflammation and emergency hematopoiesis. Cell *157*, 1175-1188.

Salmena, L., Lemmers, B., Hakem, A., Matysiak-Zablocki, E., Murakami, K., Au, P. Y., Berry, D. M., Tamblyn, L., Shehabeldin, A., Migon, E., et al. (2003). Essential role for caspase 8 in T-cell homeostasis and T-cell-mediated immunity. Genes & Development *17*, 883-895.

Schneider, A. T., Gautheron, J., Tacke, F., Vucur, M., and Luedde, T. (2015). Receptor Interacting Protein Kinase-1 (RIPK1) in hepatocytes does not mediate murine acetaminophen toxicity. Hepatology *64*, 306-308.

Schulze, K., Imbeaud, S., Letouze, E., Alexandrov, L. B., Calderaro, J., Rebouissou, S., Couchy, G., Meiller, C., Shinde, J., Soysouvanh, F., et al. (2015). Exome sequencing of hepatocellular carcinomas identifies new mutational signatures and potential therapeutic targets. Nat Genet *47*, 505-511.

Takahashi, N., Duprez, L., Grootjans, S., Cauwels, A., Nerinckx, W., DuHadaway, J. B., Goossens, V., Roelandt, R., Van Hauwermeiren, F., Libert, C., et al. (2012). Necrostatin-1 analogues: critical issues on the specificity, activity and in vivo use in experimental disease models. Cell Death & Disease *3*, e437.

Takahashi, N., Vereecke, L., Bertrand, M. J., Duprez, L., Berger, S. B., Divert, T., Goncalves, A., Sze, M., Gilbert, B., Kourula, S., et al. (2014). RIPK1 ensures intestinal homeostasis by protecting the epithelium against apoptosis. Nature *513*, 95-99.

Takeuchi, M., Rothe, M., and Goeddel, D. V. (1996). Anatomy of TRAF2. Distinct domains for nuclear factor-kappaB activation and association with tumor necrosis factor signaling proteins. The Journal of Biological Chemistry *271*, 19935-19942.

Vince, J. E., Chau, D., Callus, B., Wong, W. W., Hawkins, C. J., Schneider, P., McKinlay, M., Benetatos, C. A., Condon, S. M., Chunduru, S. K., et al. (2008). TWEAK-FN14 signaling induces lysosomal degradation of a cIAP1-TRAF2 complex to sensitize tumor cells to TNFalpha. The Journal of Cell Biology *182*, 171-184.

Vucur, M., Reisinger, F., Gautheron, J., Janssen, J., Roderburg, C., Cardenas, D. V., Kreggenwinkel, K., Koppe, C., Hammerich, L., Hakem, R., et al. (2013). RIP3 inhibits inflammatory hepatocarcinogenesis but promotes cholestasis by controlling caspase-8- and JNK-dependent compensatory cell proliferation. Cell Reports *4*, 776-790.

Vucur, M., Roderburg, C., Bettermann, K., Tacke, F., Heikenwalder, M., Trautwein, C., and Luedde, T. (2010). Mouse models of hepatocarcinogenesis: what can we learn for the prevention of human hepatocellular carcinoma? Oncotarget *1*, 373-378.

Wang, P., Zhang, J., Bellail, A., Jiang, W., Hugh, J., Kneteman, N. M., and Hao, C. (2007). Inhibition of RIP and c-FLIP enhances TRAIL-induced apoptosis in pancreatic cancer cells. Cellular Signalling *19*, 2237-2246.

Weinlich, R., and Green, D. R. (2014). The two faces of receptor interacting protein kinase-1. Molecular Cell *56*, 469-480.

Wilson, N. S., Dixit, V., and Ashkenazi, A. (2009). Death receptor signal transducers: nodes of coordination in immune signaling networks. Nature Immunology *10*, 348-355.

Wong, W. W., Gentle, I. E., Nachbur, U., Anderton, H., Vaux, D. L., and Silke, J. (2010). RIPK1 is not essential for TNFR1-induced activation of NF-kappaB. Cell Death and Differentiation *17*, 482-487.

FIGURE LEGENDS

Figure 1. Normal Liver Development and Homeostasis in RIPK1^{LPC-KO} Mice.

(A)   Gene targeting strategy for the generation of mice with conditional deletion of *Ripk1* in liver parenchymal cell (LPC). A targeting vector containing an *frt*-flanked (white triangle) lacZ operon and neomycin resistance cassette (neo) as well as *loxP*-flanked (black arrow head) Exons 4 and 5 of the *Ripk1* genomic locus was used to generate the targeted locus in embryonic stem cells via homologous recombination. Cross-breeding of mice bearing the modified *Ripk1* locus with Flp expressing mice led to the removal of neo and lacZ. Subsequent cross-breeding with alfp-Cre-positive mice led to the disruption of *Ripk1* in LPC (RIPK1^{LPC-KO}).

(B)   PCR analysis of genomic DNA isolated from tails of WT (+/+), heterozygous (+/p), and homozygous RIPK1^{LPC-KO} (p/p) mice.

(C)   Western blot analysis on whole liver extracts and primary hepatocyte extracts from 6-week-old RIPK1^{LPC-KO} and control littermate (WT) mice.

(D)   Serum level analysis of aspartate aminotransferase (AST), alanine aminotransferase (ALT) and glutamate dehydrogenase (GLDH) in 6-week-old (n = 6) and 50-week-old mice (n = 5). Results are shown as mean. n.s. = not significant.

(E)   Histological analysis of liver paraffin sections from 6-week-old and 50-week-old WT and RIPK1^{LPC-KO} mice.

        See also Figure S1.

Figure 2. *Ripk1* Ablation Promotes LPS/TNF-Dependent Hepatocyte Apoptosis and Liver Damage Independently of NF-κB.

(A)   Analysis of serum levels of AST, ALT and GLDH after 8 hr of LPS stimulation from 6-week-old WT and RIPK1^{LPC-KO} mice. Results are shown as mean. *$p < 0.05$; **$p < 0.01$; ***$p < 0.001$ (n = 6).

(B)   Representative H/E staining and cl. Caspase-3 staining on liver slides from 6-week-old WT and RIPK1^{LPC-KO} mice at 8 hr after LPS injection.

(C)   Western blot analysis on liver extracts from WT and RIPK1^{LPC-KO} mice treated with LPS for different time points.

(D)   Electrophoretic mobility shift assay (EMSA) on nuclear extracts from primary hepatocytes of WT and RIPK1^{LPC-KO} mice stimulated with TNF for different time points. Antibodies against the NF-κB subunits p50 (lane 1) and p65 (lane 2) were added as supershift controls.

(E)   Induction of the NF-κB target-genes *A20* and *IκBa* in response to TNF stimulation was examined in primary hepatocytes isolated from WT and RIPK1^{LPC-KO} mice by qRT-PCR. Results are expressed as mean, +/- SEM. ***$p < 0.001$ (n = 6).

See also Figure S2.

Figure 3. *Ripk1*-Deficiency Promotes Activation of Caspase-8 and an Early Pro-Apoptotic Function of RIPK3 in Hepatocytes.

(A)   Analysis of serum levels of AST, ALT and GLDH after 8 hr of LPS stimulation from 6-week-old WT, RIPK1^{LPC-KO}, RIPK1/Caspase-8^{LPC-KO} and RIPK1^{LPC-KO}/RIP3$^{-/-}$ mice. Results are shown as mean. ns = not significant (n = 6).

(B, C) Representative H/E and cl. Caspase-3 stainings (B) and TUNEL assay (C) of liver slides from 6-week-old mice untreated or stimulated for 4 hr and 8 hr with LPS. Arrow heads indicate focal hepatocellular injury.

(D, E) Statistical analysis of cl. Caspase-3$^+$ (D) and TUNEL$^+$ (E) hepatocytes on liver slides from mice treated with LPS for 4 hr and 8 hr. Results are shown as mean. ***$p < 0.001$ (n = 6).

(F, G) Western blot analysis on liver extracts from the indicated 6-week-old mice treated with LPS for different time points. * = nonspecific band.

See also Figure S3.

Figure 4. Loss of *Ripk1* Promotes TRAF2 Degradation in a Kinase-Independent Manner.

(A)   HepG2 lysates were stimulated with Fc-TNF for 5 min, followed by precipitation of the Fc-tag via Agarose G beads. In non-stimulated extracts, Fc-TNF was added as control after cell lysis and precipitated overnight. Western blot analyses were performed after precipitation for the indicated proteins (left panel). Expression of the respective proteins in straight lysates was shown to control for input (right panel). pUb = polyubiquitinated.

(B)   Western blot analysis of extracts from LPS-treated livers and soluble and insoluble fractions of TNF-treated primary hepatocytes from WT and RIPK1[LPC-KO] mice.

(C)   Western blot analysis on Fas-Ligand-treated primary hepatocytes from WT and RIPK1[LPC-KO] mice.

(D)   Western blot analysis on primary hepatocytes from WT and RIPK1[LPC-KO] mice treated with TNF for the indicated time points in the absence or presence of the proteasomal inhibitor Bortezomib. Soluble and insoluble fractions were analyzed.

(E)   Western blot analysis of primary hepatocytes from WT and RIPK1[LPC-KO] mice treated with TNF for the indicated time points. Necrostatin-1s was added 1 hr prior to TNF stimulation. * = nonspecific band.

(F)   Western blot analysis on extracts from whole liver and from primary hepatocytes of WT, RIPK1[KD] and RIPK1[LPC-KO] mice treated with LPS or TNF respectively for the indicated time points.

See also Figure S4.

Figure 5. Spontaneous Hepatitis and Cholestasis Upon Combined Ablation of *Ripk1* and *Traf2* in LPC.

(A)   Western blot analysis on liver extracts from 6-week-old mice.

(B)   Representative macroscopic pictures of livers from 6-week-old mice. Livers of RIPK1/TRAF2[LPC-KO] mice showed multiple small nodules and an icteric color.

(C)   Serum level analysis of AST, ALT, GLDH and alkaline phosphatase (AP) in 6-week-old mice. Results are shown as mean. ***$p < 0.001$; n.s. = not significant (n = 6).

(D)   Histological analysis of liver sections obtained from mice at 6 weeks of age. Areas of hepatocellular dysplasia are indicated in RIPK1/TRAF2[LPC-KO] livers.

(E)   Immunohistochemical (IHC) staining and quantification of cl. Caspase-3[+] and Ki67^{+} hepatocytes in the respective 6-week-old mice. Results are shown as mean. **$p < 0.01$; ***$p < 0.001$; n.s. = not significant (n = 6).

(F)   Western blot analysis of liver extracts from 6-week-old WT, RIPK1[LPC-KO], TRAF2[LPC-KO] and RIPK1/TRAF2[LPC-KO] mice.

(G, H) Representative IHC staining (G) and quantification (H) of RelA/p65[+] hepatocytes of 6-week-old WT and RIPK1/TRAF2[LPC-KO] mice untreated or stimulated for 1 hr and 2 hr with LPS. Results are expressed as mean, +/- SEM. ***$p < 0.001$ (n = 5).

(I)   EMSA analysis on nuclear extracts from primary hepatocytes of WT and RIPK1/TRAF2[LPC-KO] mice stimulated with TNF for different time points. Antibodies against the NF-κB subunits p50 (lane 1) and p65 (lane 2) were added as supershift controls.

(J)   Induction of the NF-κB target genes *A20* and *IκBa* in response to TNF stimulation was examined in primary hepatocytes isolated from WT and RIPK1/TRAF2[LPC-KO] mice by qRT-PCR. Results are expressed as mean, +/- SEM. *$p < 0.05$; ***$p < 0.001$; n.s. = not significant (n = 6).

See also Figure S5.

Figure 6. RIPK1 and TRAF2 Collaborate to Prevent Caspase-8-Dependent Hepatocarcinogenesis in RIPK1/TRAF2[LPC-KO] Mice.

(A)   Representative macroscopic pictures of 50-52-week-old mice. RIPK1/TRAF2[LPC-KO] mice displayed multiple large liver tumors.

(B)   Liver-weight / body-weight ratio of RIPK1/TRAF2[LPC-KO] mice compared to the other indicated genotypes. Results are shown as mean. ***$p < 0.001$ (n = 5).

(C)   H/E and Collagen IV staining of liver sections from 50-52-week-old mice. Only RIPK1/TRAF2^{LPC-KO} mice displayed HCC. Note the loss of Collagen IV fibers in HCC tissue.

(D)   Serum level analysis of AST, ALT and GLDH in 6-week-old mice. Results are shown as mean. n.s. = not significant (n = 5).

(E)   Representative macroscopic pictures of 6-week-old and 52-week-old mice.

(F)   H/E staining of representative liver sections from the indicated 6-week-old and 52-week-old mice.

(G)   Western blot analysis of liver extracts from WT and RIPK1/TRAF2/Casp-8^{LPC-KO} mice. See also Table S1 and Figure S6.

Figure 7. TRAF2/IKKβ^{LPC-KO} Mice Develop Adenomatous Hyperplasia, Dysplastic Foci and HCC.

(A)   Western blot analysis on liver extracts from 6-week-old mice.

(B)   EMSA analysis on nuclear extracts from primary hepatocytes of WT and TRAF2/IKKβ^{LPC-KO} mice stimulated with TNF for different time points. Antibodies against the NF-κB subunits p50 (lane 1) and p65 (lane 2) were added as supershift controls.

(C)   Representative macroscopic pictures of livers from 6-week-old mice.

(D)   Serum level analysis of AST, ALT and GLDH in 6-week-old mice. Results are shown as mean. **$p < 0.01$; ***$p < 0.001$ (n = 6).

(E)   H/E and IHC staining and quantification of cl. Caspase-3$^+$ and Ki67$^+$ hepatocytes in the respective 6-week-old mice. Results are shown as mean. ***$p < 0.001$ (n = 6).

(F)   Representative macroscopic pictures of 52-week-old mice.

(G)   H/E staining of liver sections from 52-week-old WT and TRAF2/IKKβ^{LPC-KO} mice.

(H)   Proposed model on the roles of RIPK1 and TRAF2 in preventing liver injury upon TNF stimulation and spontaneous hepatocarcinogenesis. Liver pictures were taken from Figures 6A and 7F.

See also Table S1 and Figure S7.

Figure 8. Association of the Expression of RIPK1 and TRAF2 in Human HCCs with Patients' Prognosis.

(A)   Representative IHC stainings of human liver sections from HCC-patients. Staining was performed on a tissue microarray (TMA). Examples for negative [immunoreactive (IR)-score <2] and positive stainings (IR-score =2 and IR-score > 2) are depicted.

(B)   Kaplan-Meier curves for the overall survival of HCC-patients plotted against time in months for different subgroups based on RIPK1 expression levels in HCC sections.

(C)   Distribution of RIPK1 expression according to IR-scores along the collective of HCC samples.

(D)   Kaplan-Meier curves for the overall survival of HCC-patients plotted against time in months for different subgroups based on TRAF2 expression levels in HCC sections.

(E)   Distribution of TRAF2 expression according to IR-scores along the collective of HCC samples.

 (F, G) Kaplan-Meier curves for the overall survival of HCC-patients plotted against time in months for different subgroups based on combined RIPK1/TRAF2 expression levels in HCC sections (F). All technically evaluable samples were included into this analysis. Stainings were evaluated using the IR-score and correlated with the survival of the patients. To assess the relationship between the combined RIPK1/TRAF2 expression levels, a combined-score (CS) was generated (G).
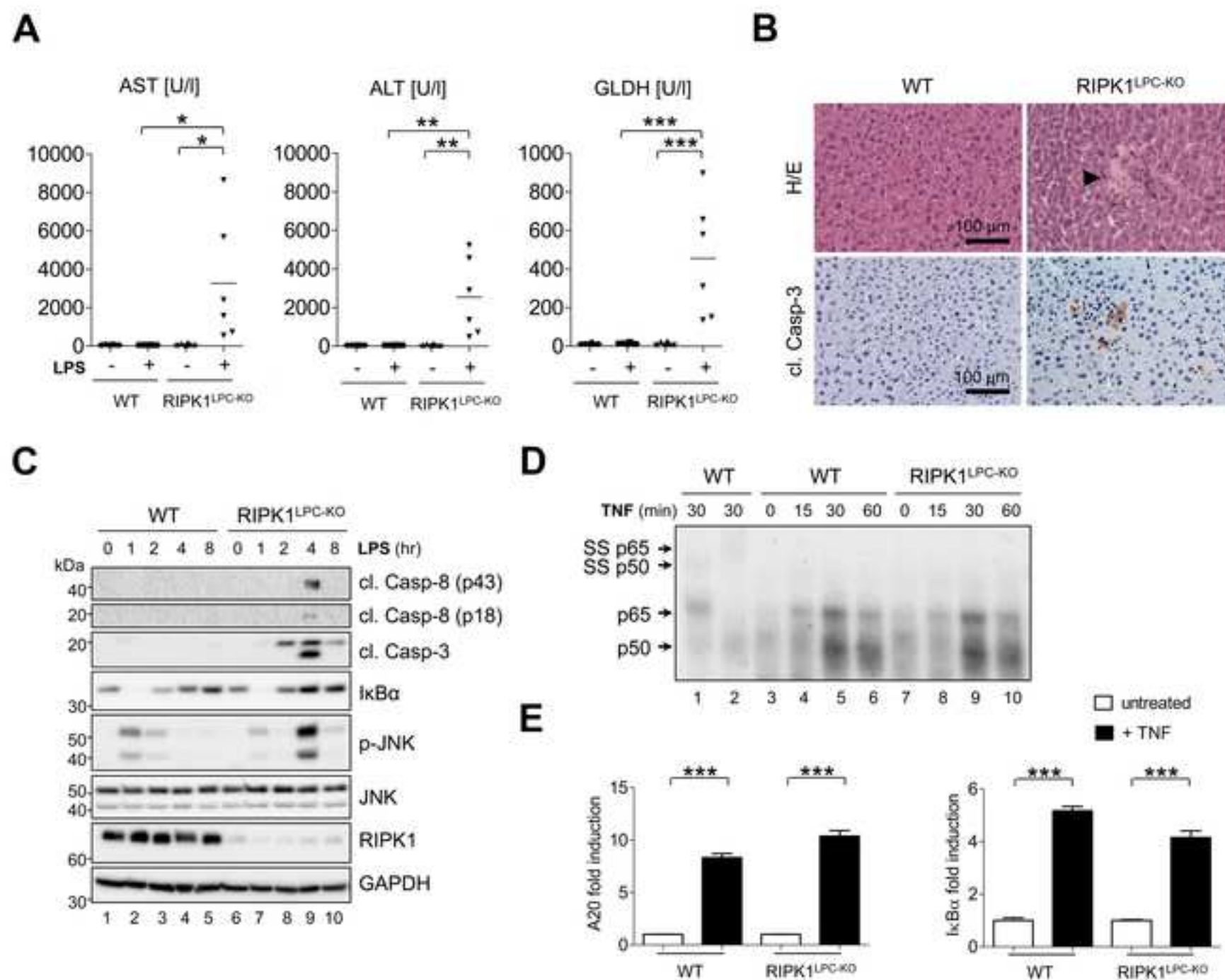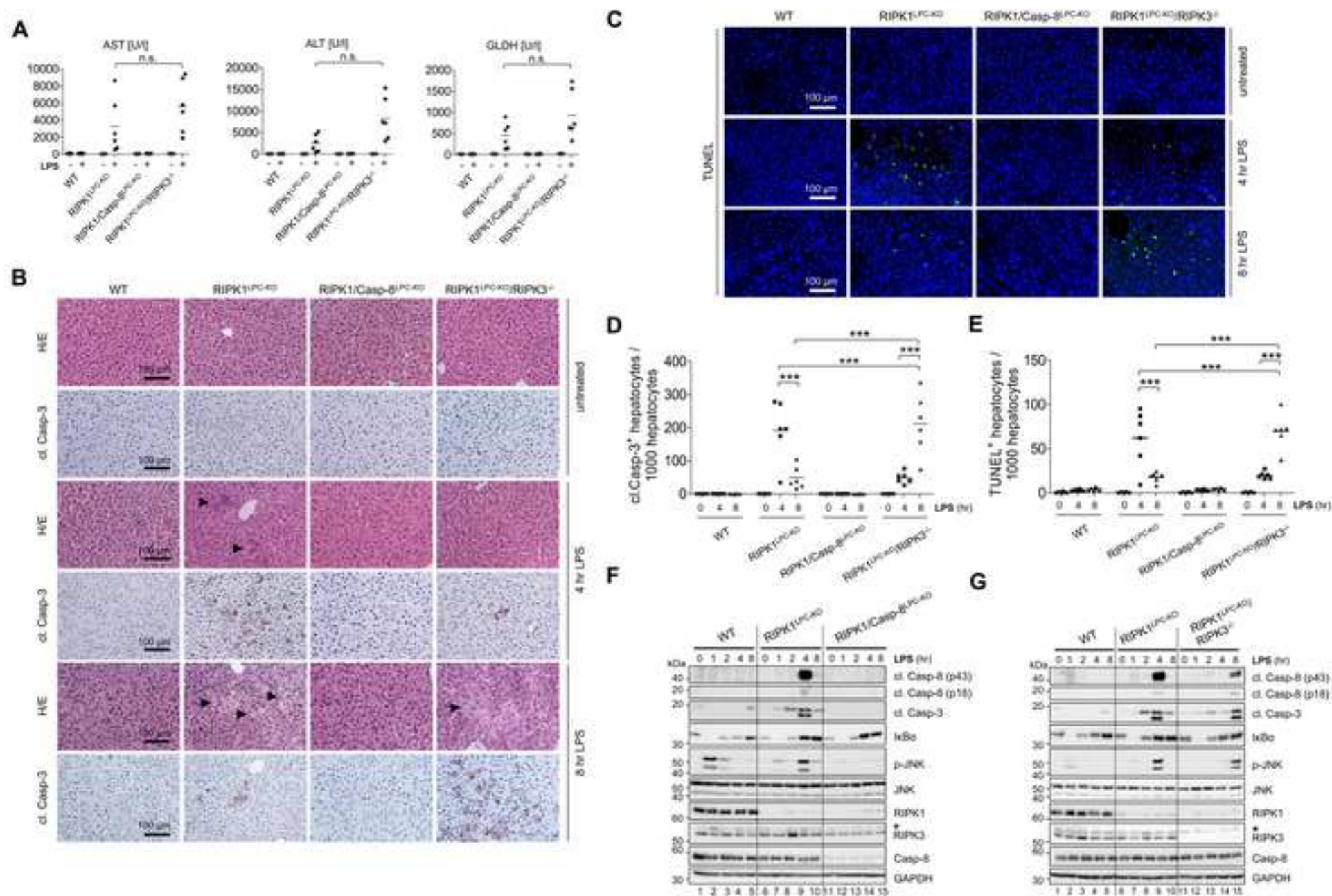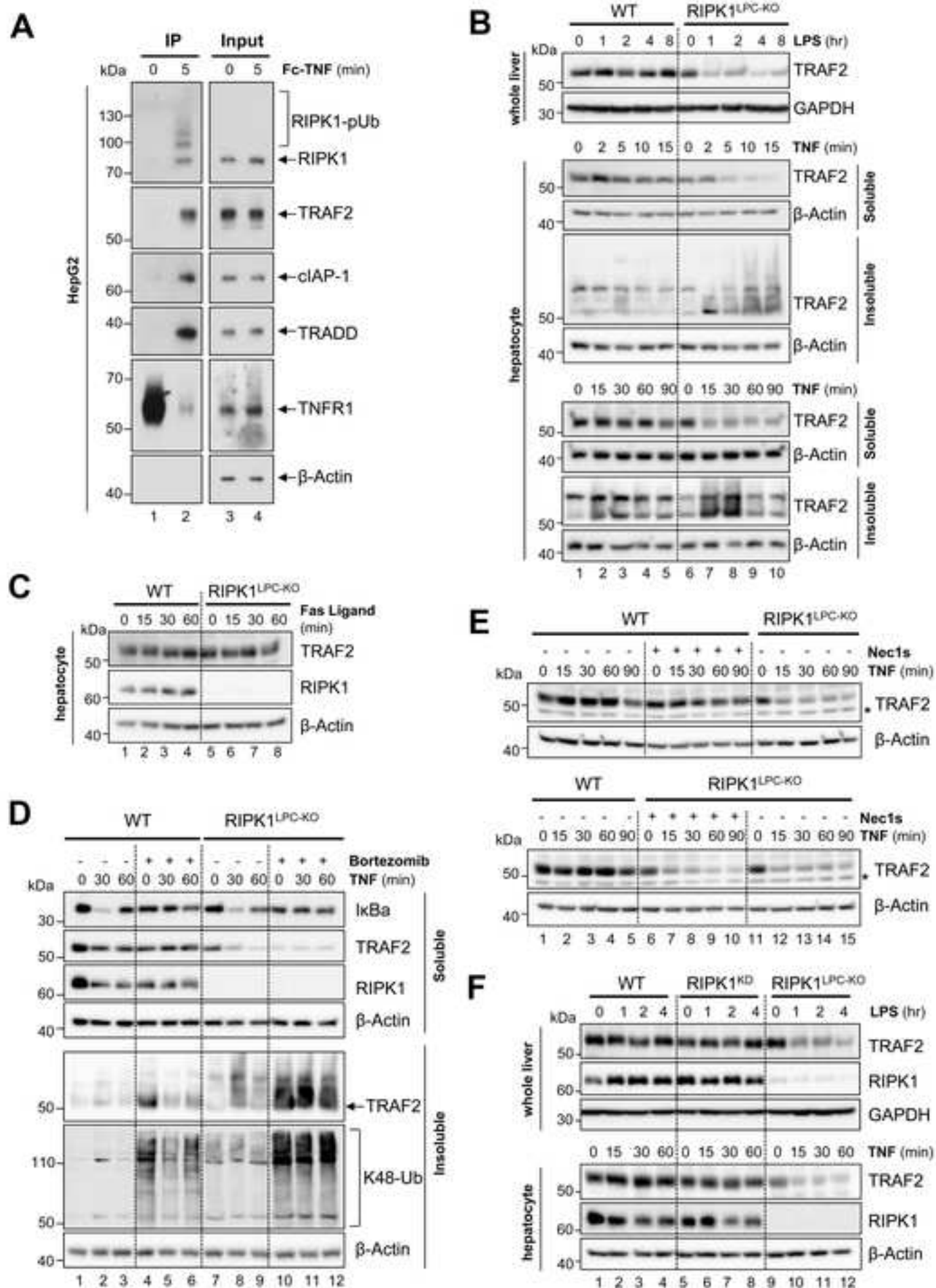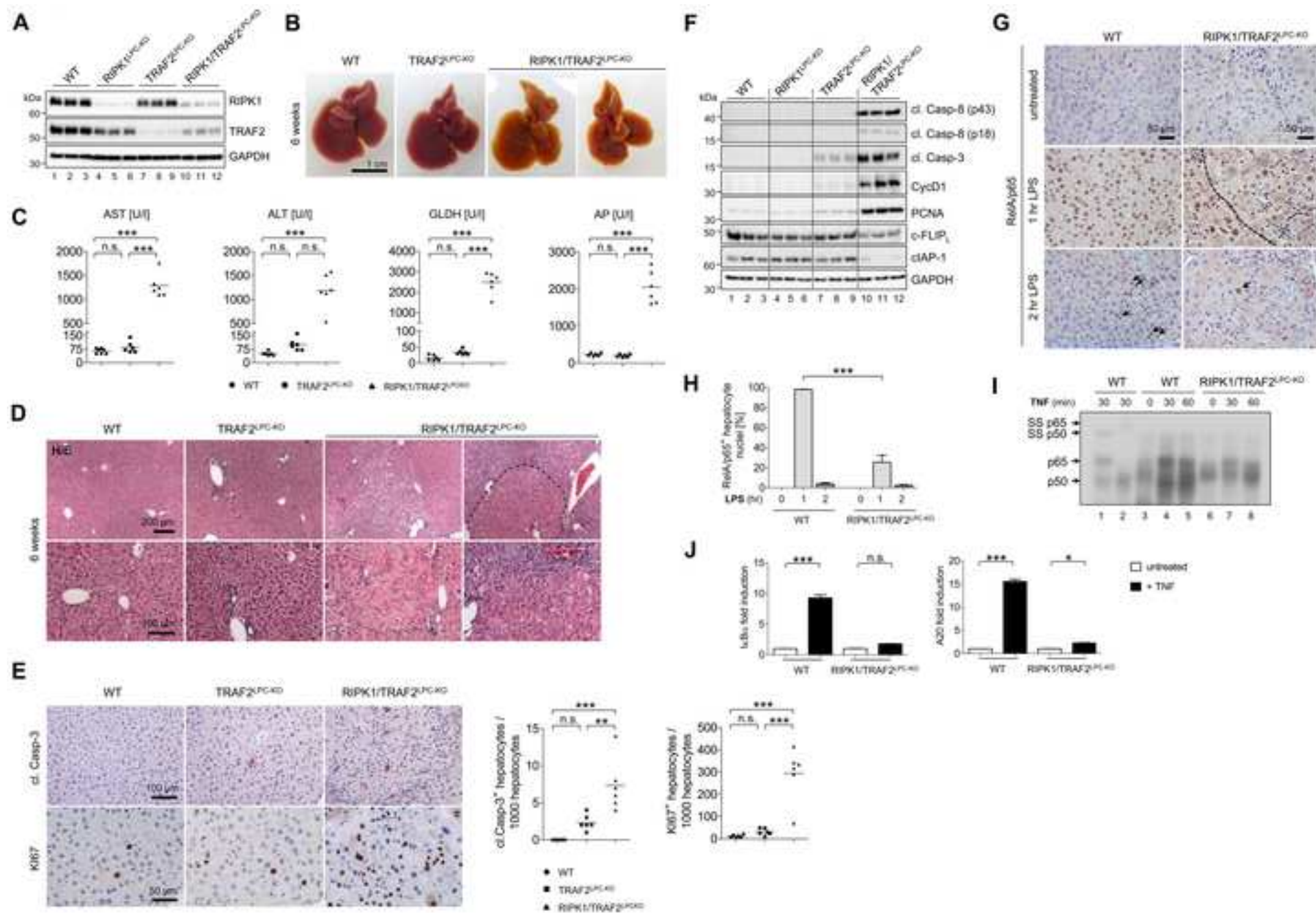
See also Table S2.

Figure 1　　　　　　　　　　　　　　　　　　　　Click here to download Figure Figure 1.tif ±

Figure 2

Click here to download Figure Figure 2.tif ⬇

Figure 3

Figure 4

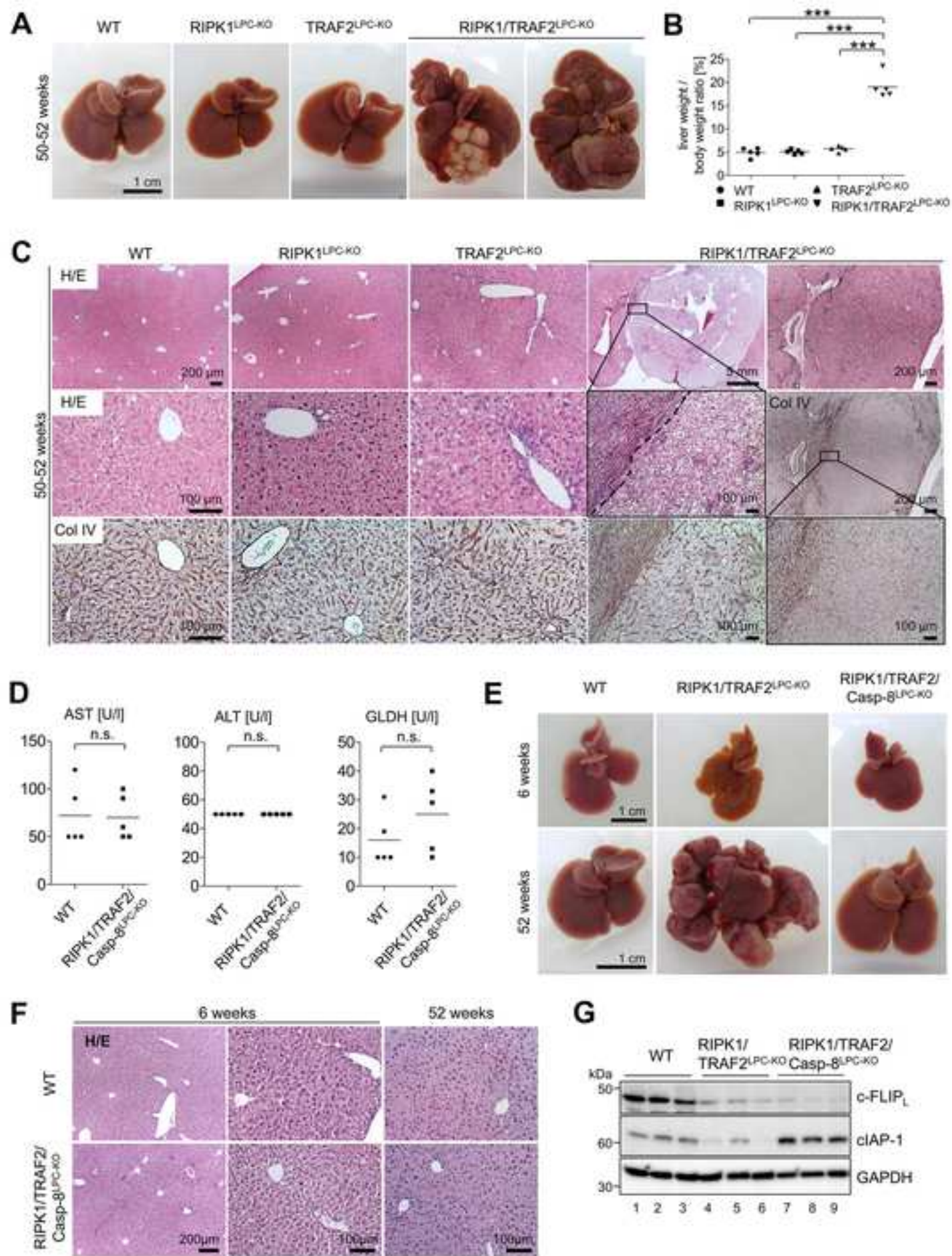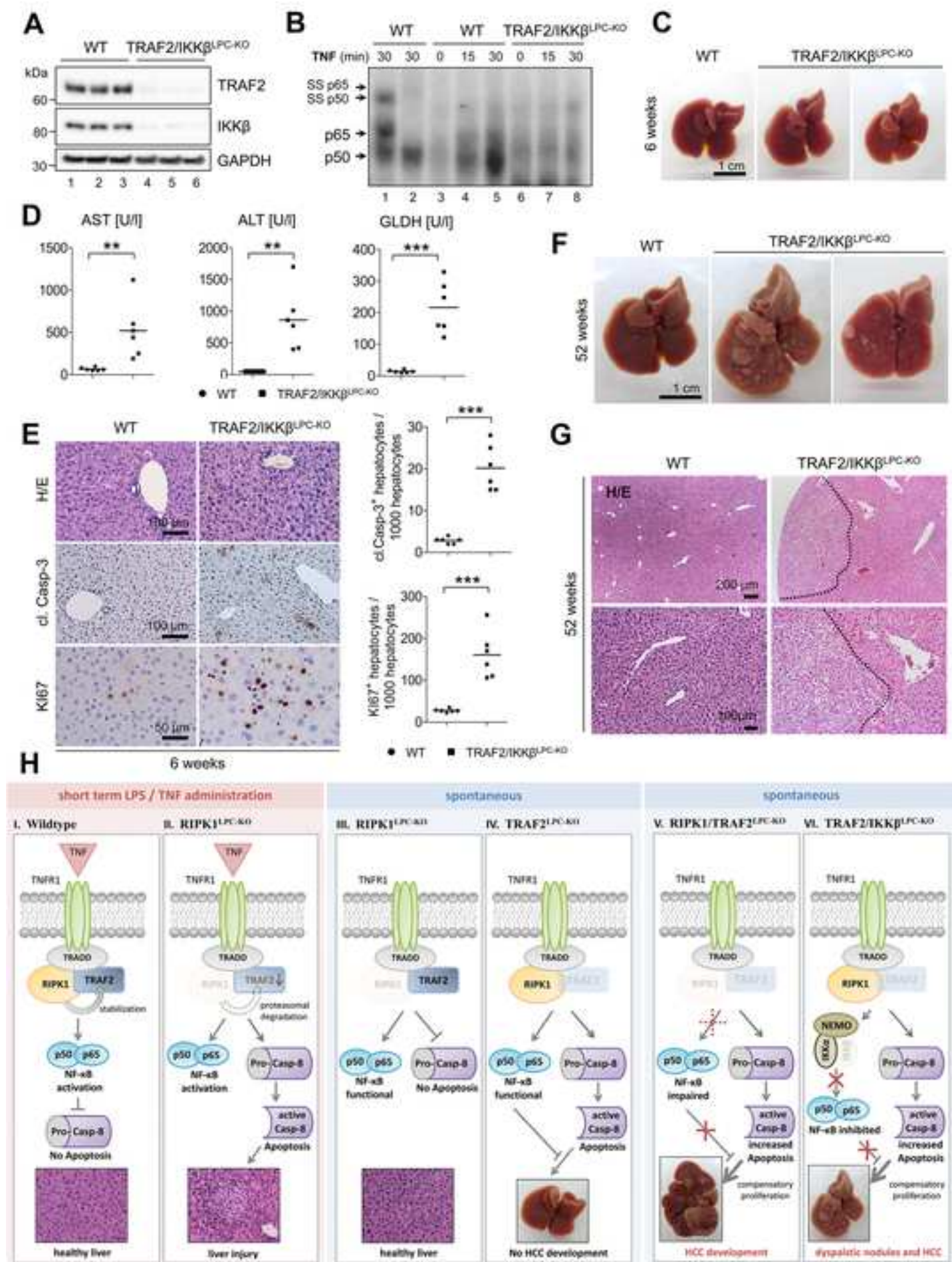Click here to download Figure figure 4.tif ⬇
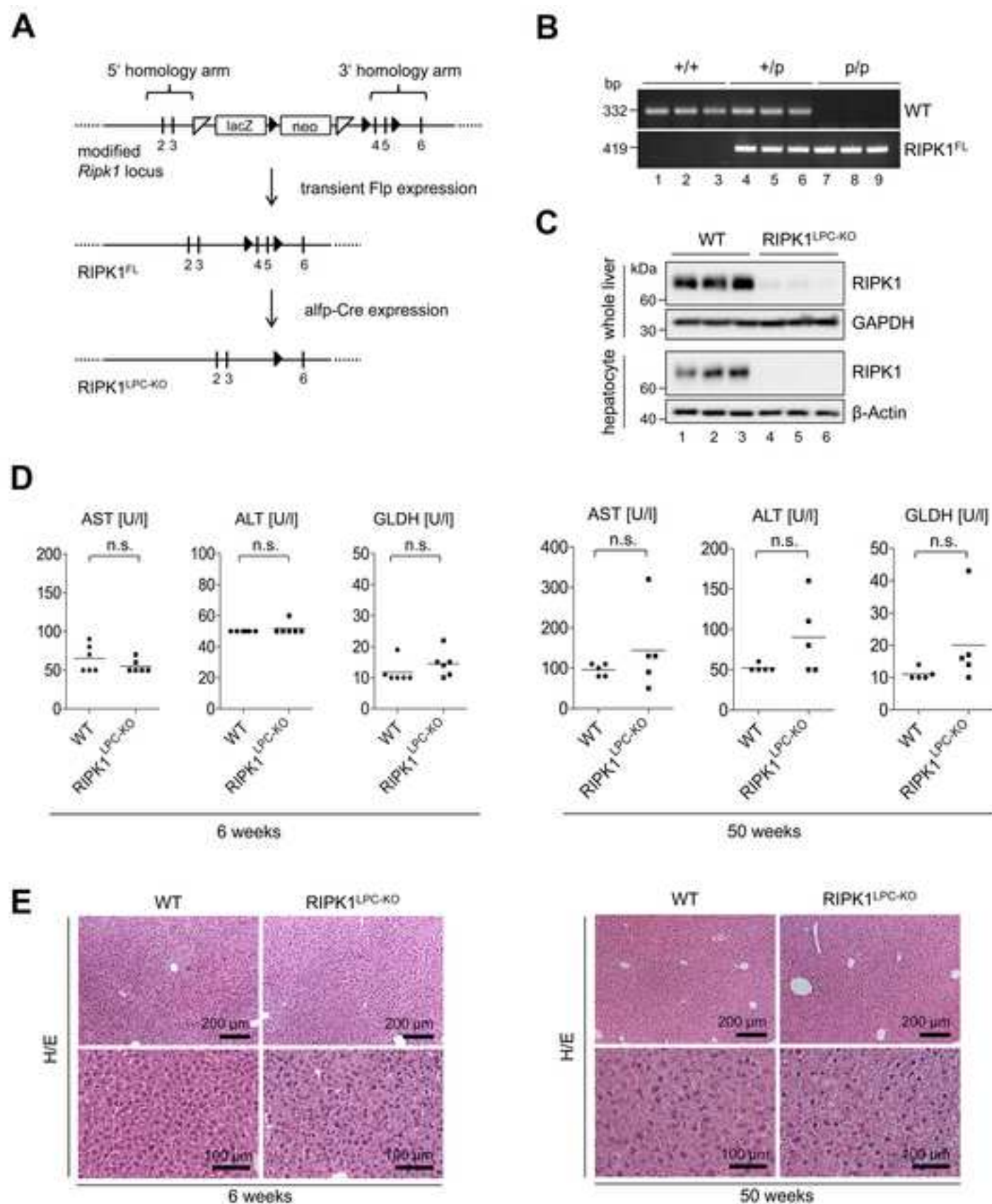
Figure 5

Figure 7

Figure 8

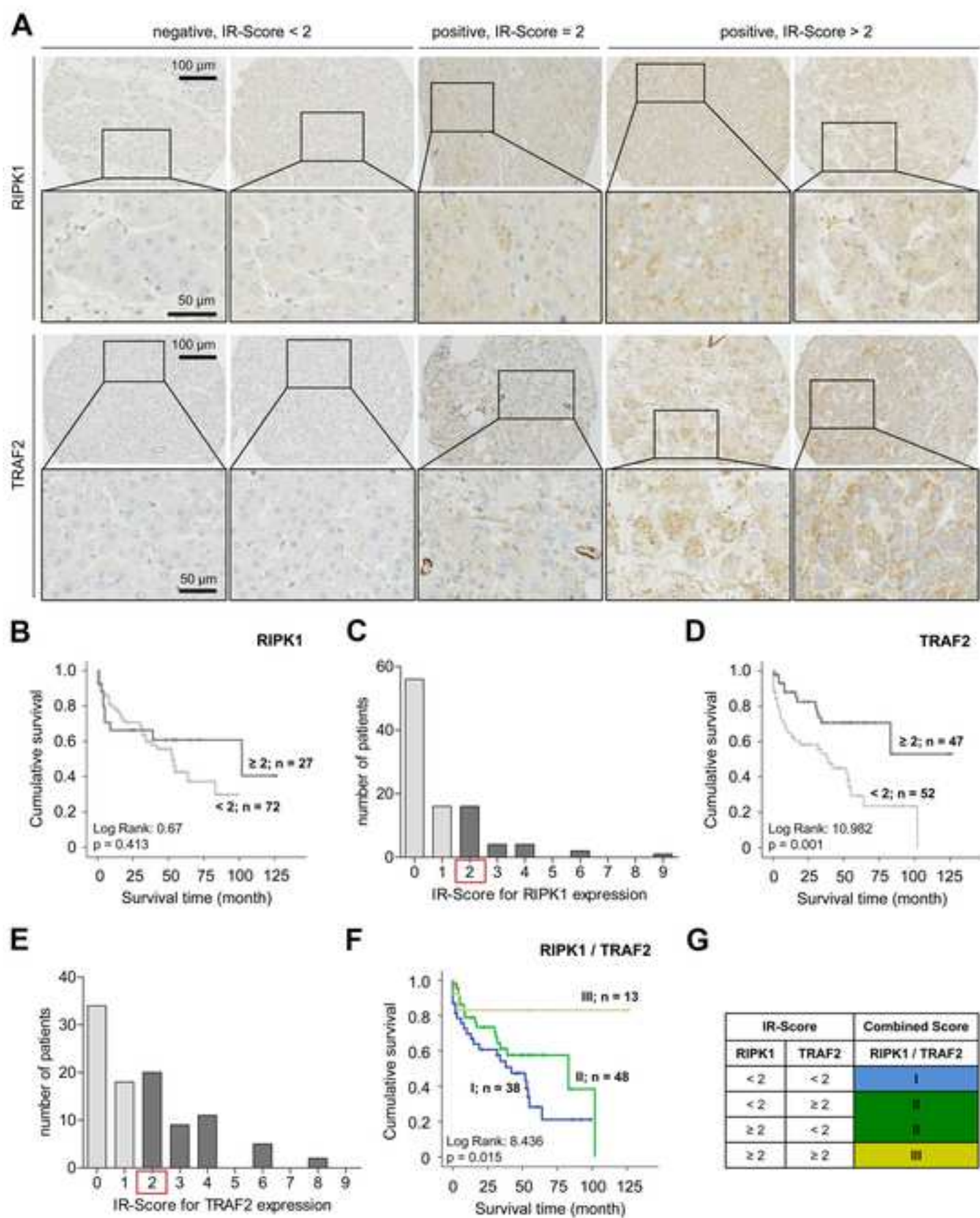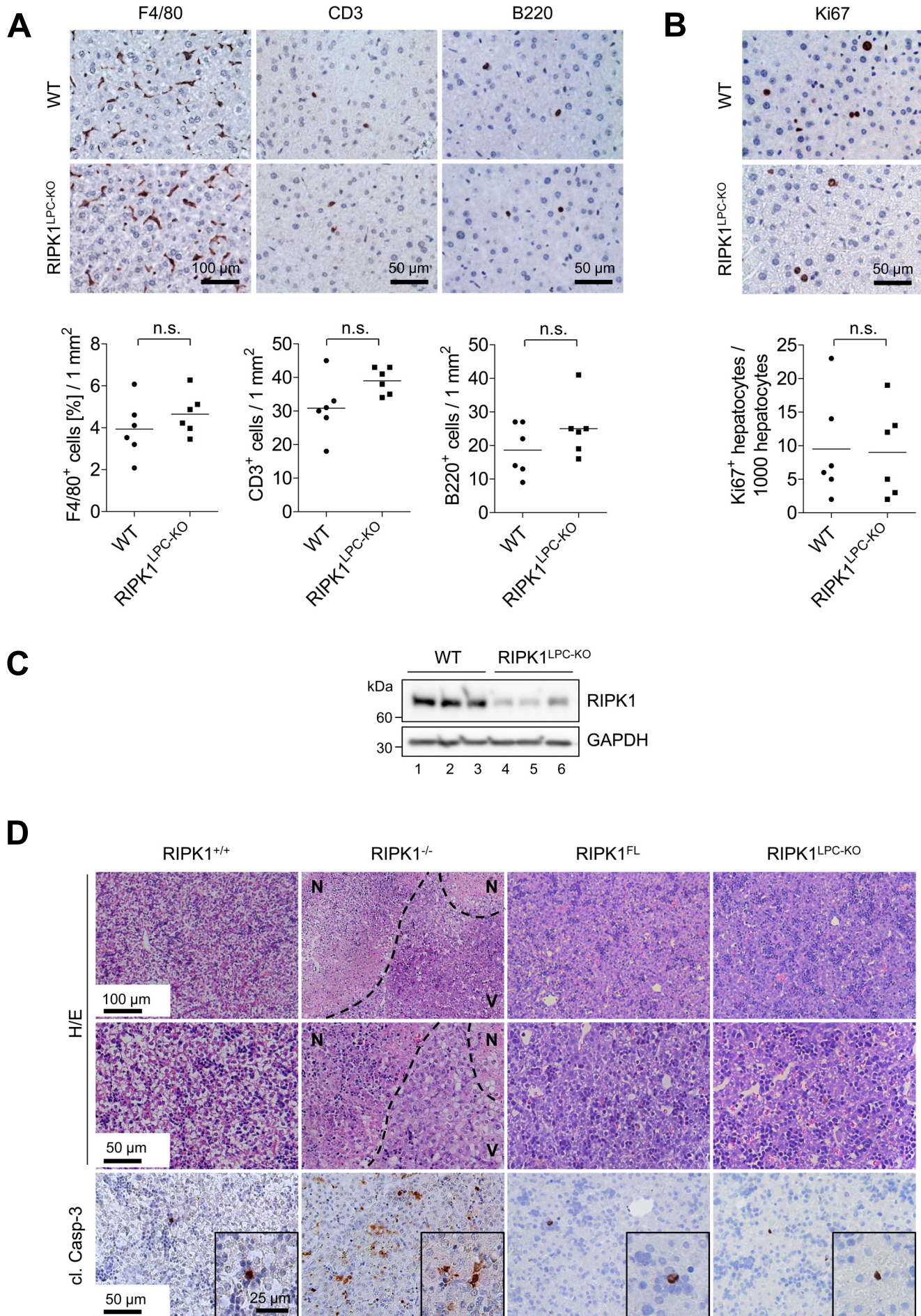Click here to download Figure figure 8.tif

Figure S1, related to Figure 1. Comparison between perinatal RIPK1^{LPC-KO} and RIPK1^{-/-} mice.
(**A,B**) Immunohistochemical (IHC) (upper panel) and statistical (lower panel) analysis of F4/80$^+$, CD3$^+$, B220$^+$ (**A**) and Ki67$^+$ (**B**) liver cells on representative liver sections from 6-week-old WT and RIPK1^{LPC-KO} mice. Results are shown as mean. n.s. = not significant (n = 6). (**C**) Western blot analysis on whole liver extracts from one day old RIPK1^{LPC-KO} and control littermate (WT) neonates. (**D**) Representative H/E and cl. Caspase-3 stainings on liver slides from RIPK1$^{+/+}$, RIPK1$^{-/-}$, RIPK1^{FL} and RIPK1^{LPC-KO} mice, which were all sacrificed perinatally. N = necrotic area, V = viable area.
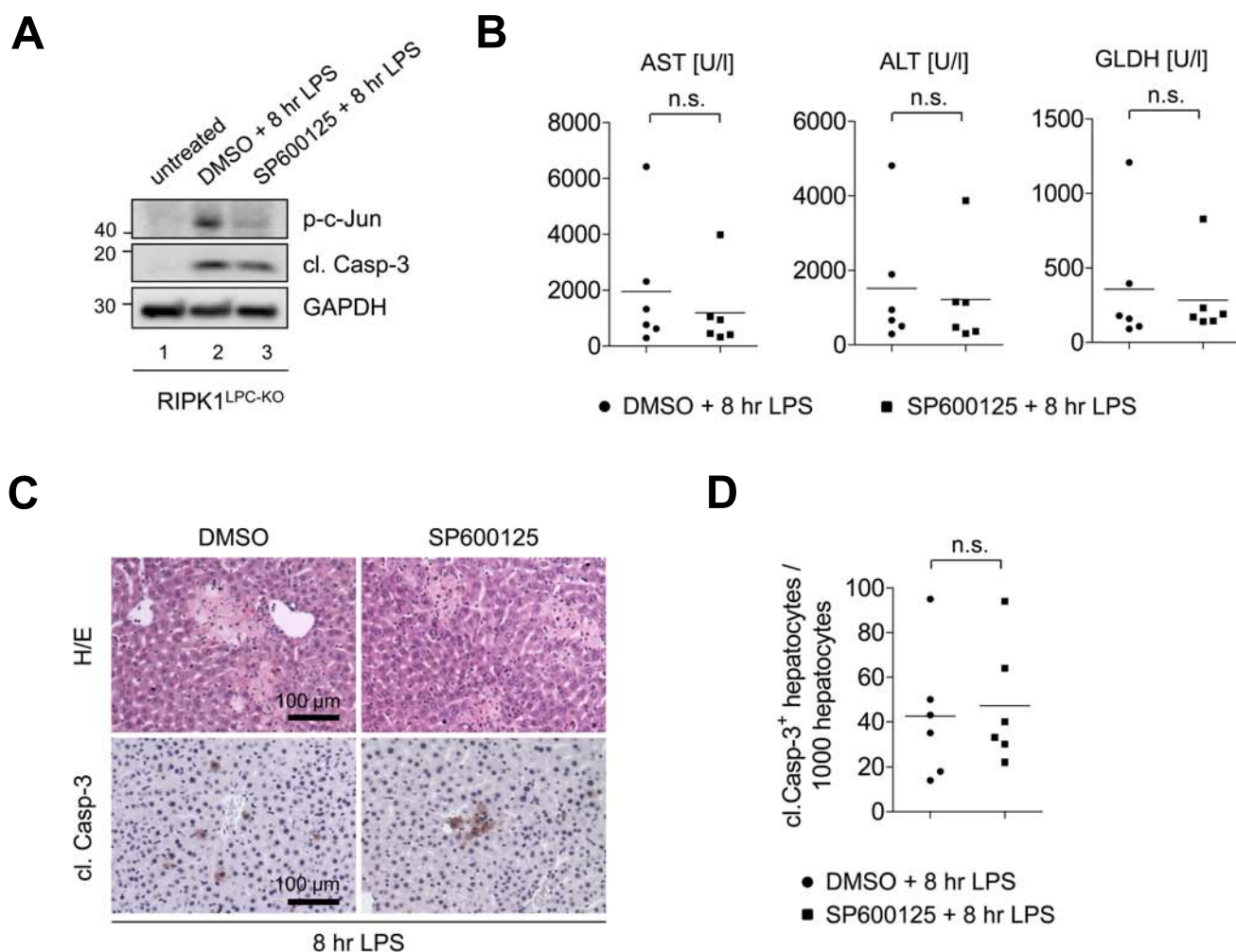
Figure S2, related to Figure 2. Liver injury and cell death in RIPK1^LPC-KO mice are independent of JNK activation.
(**A**) Western blot analysis of liver extracts from 6-week-old RIPK1^LPC-KO mice stimulated with LPS for 8 hr and pre-treated with the JNK-inhibitor SP600125 or vehicle (DMSO). (**B**) Serum level analysis of AST, ALT and GLDH of LPS treated RIPK1^LPC-KO mice pre-treated with SP600125 or DMSO. Results are shown as mean. n.s. = not significant (n = 6). (**C+D**) H/E and IHC staining (**C**) and quantification of cl. Caspase-3⁺ hepatocytes (**D**) on liver slides from LPS treated RIPK1^LPC-KO mice pre-treated with SP600125 or DMSO. Results are shown as mean. n.s. = not significant (n = 6).
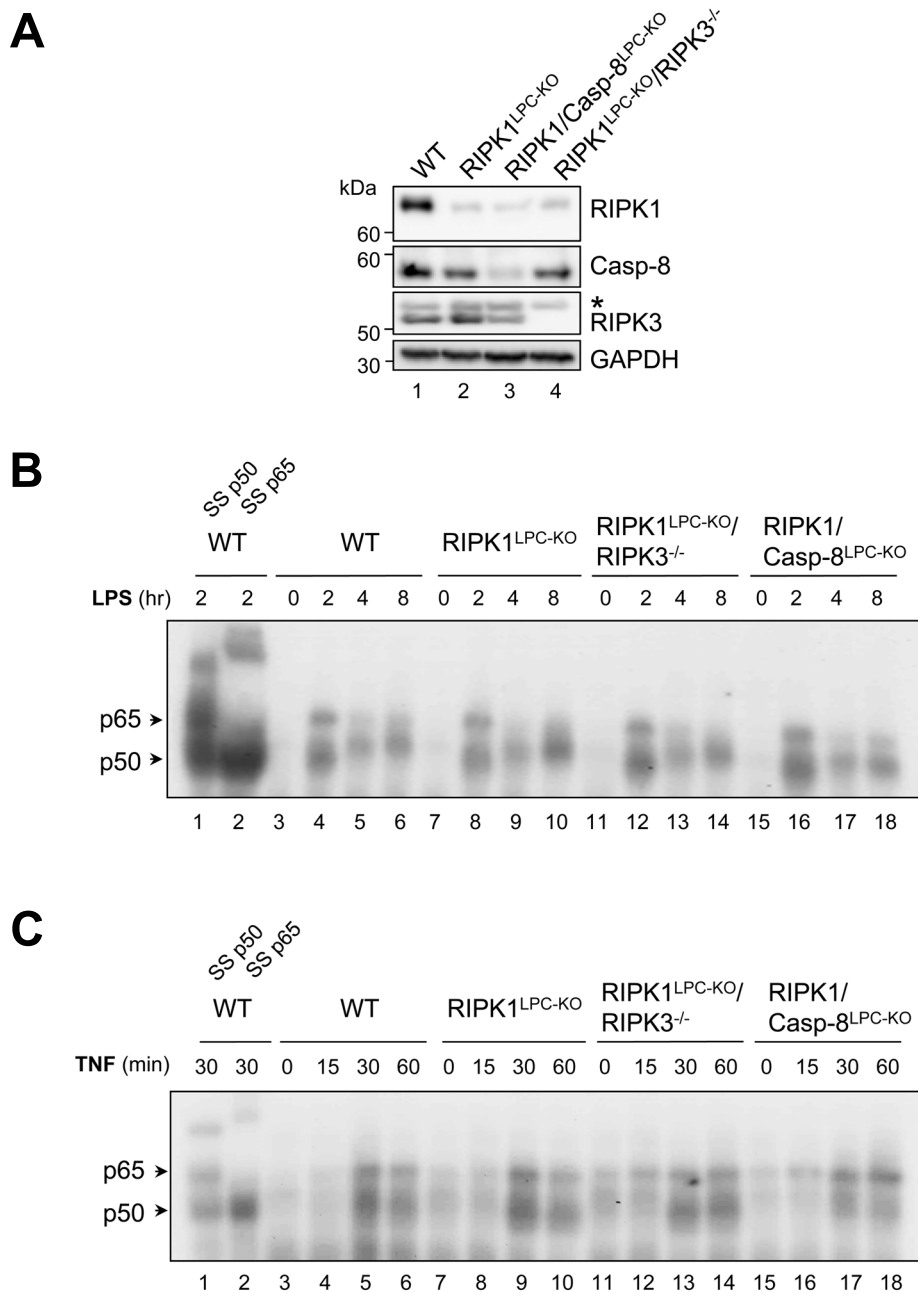
Figure S3, related to Figure 3. Additional ablation of *Caspase-8* or *Ripk3* did not change the competence of *Ripk1*-deficient hepatocytes to activate NF-κB.
(**A**) Western blot analysis on liver extracts from 6-week-old WT, RIPK1[LPC-KO], RIPK1/Caspase-8[LPC-KO] and RIPK1[LPC-KO]/RIP3^{-/-} mice. * = nonspecific band. (**B**) EMSA analysis on liver nuclear extracts from WT, RIPK1[LPC-KO], RIPK1[LPC-KO]/RIP3^{-/-} and RIPK1/Caspase-8[LPC-KO] mice treated with LPS for different time points. Antibodies against the NF-κB subunits p50 (lane 1) and p65 (lane 2) were added as supershift controls. (**C**) EMSA analysis on nuclear extracts from primary hepatocytes of WT, RIPK1[LPC-KO], RIPK1[LPC-KO]/RIP3^{-/-} and RIPK1/Caspase-8[LPC-KO] mice treated with TNF for different time points. Antibodies against the NF-κB subunits p50 (lane 1) and p65 (lane 2) were added as supershift control.
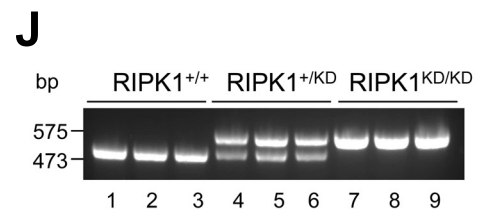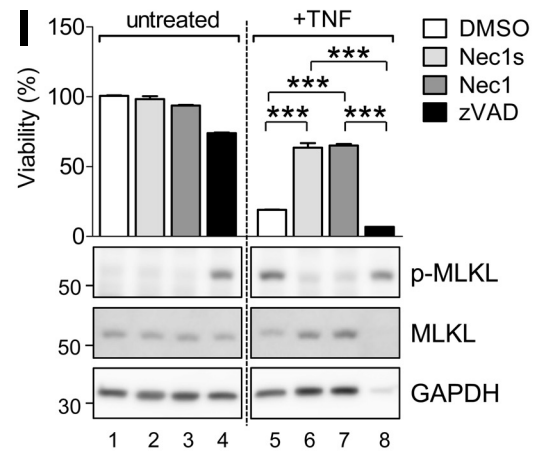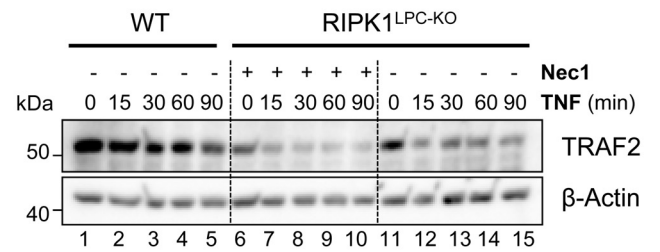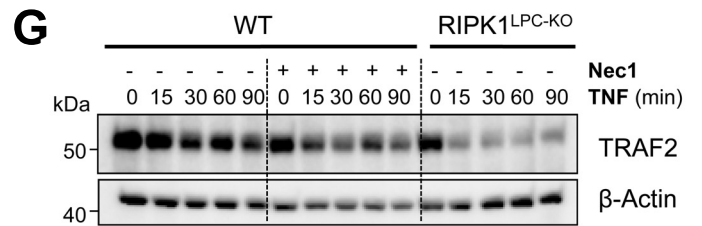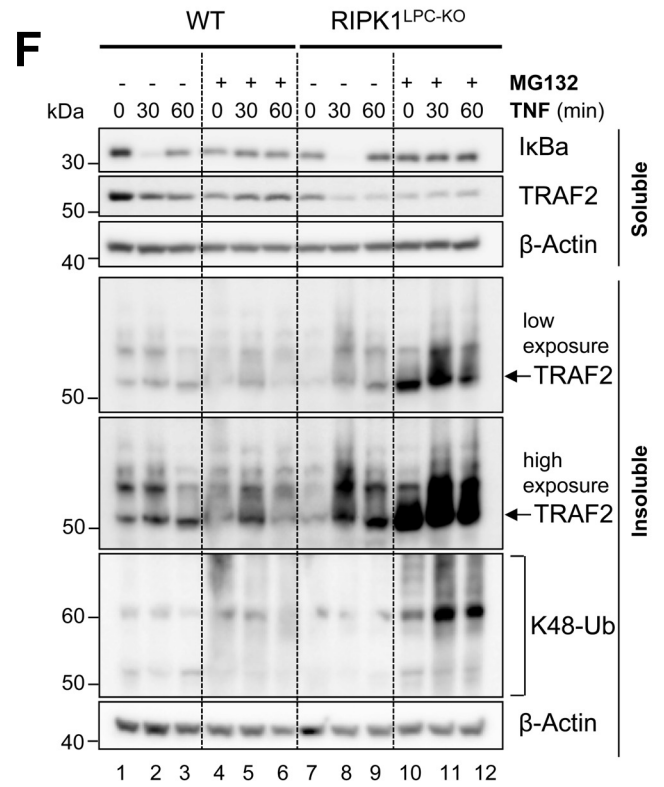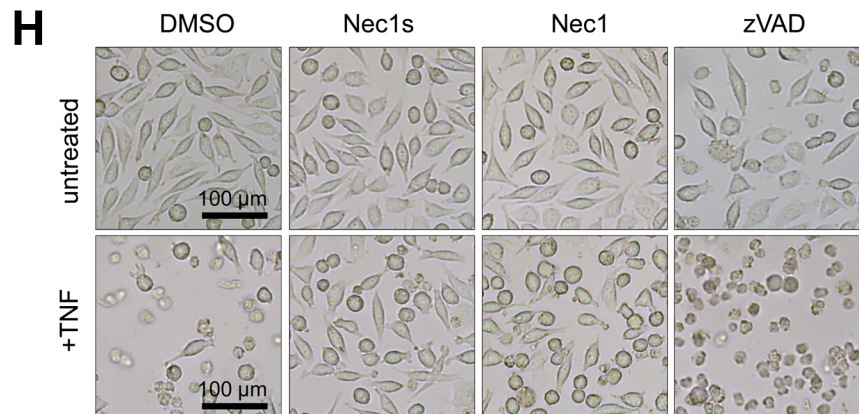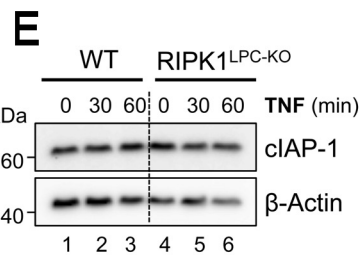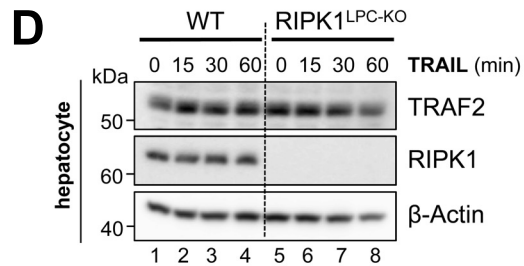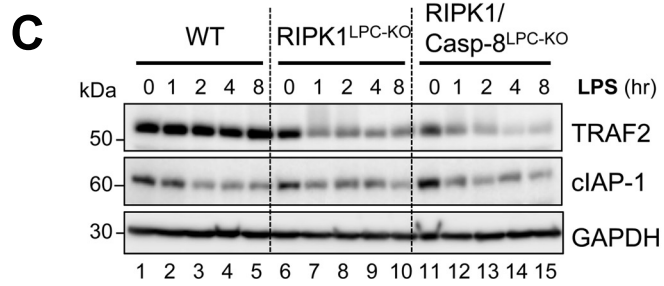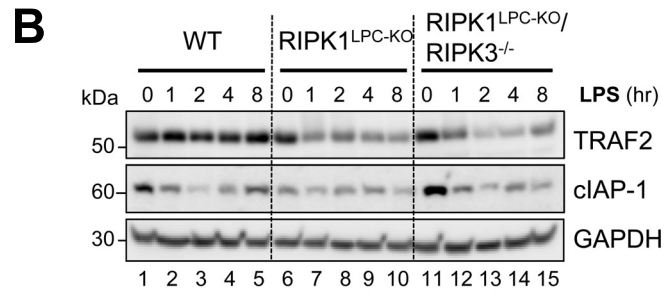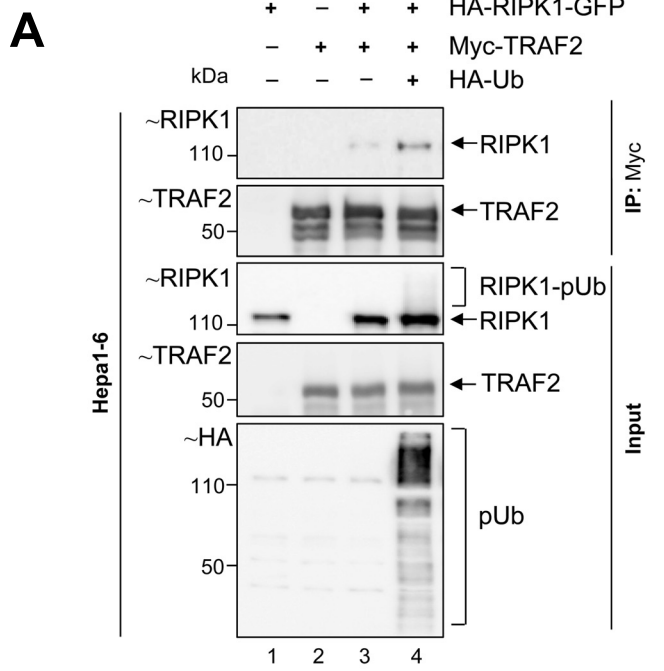
Figure S4, related to Figure 4. Loss of RIPK1 destabilizes TRAF2 expression in a kinase-activity-independent manner.

(**A**) Hepa1-6 cells were transfected alone or in combination with expression vectors coding for myc-tagged TRAF2, HA-tagged RIPK1-GFP and HA-tagged ubiquitin. Lysates were immunoprecipitated with an anti-Myc-antibody, followed by Western blot analysis for the indicated proteins (top panel). Expression of the respective proteins was shown by Western blot analysis (bottom panel). pUb = poly-ubiquitinated. (**B-C**) Western blot analysis on liver extracts of 6-week-old WT, RIPK1^{LPC-KO} and RIPK1^{LPC-KO}/RIP3$^{-/-}$ (**B**) or RIPK1/Caspase-8^{LPC-KO} (**C**) mice treated with LPS for the indicated time points. (**D**) Western blot analysis on TRAIL-treated primary hepatocytes from WT and RIPK1^{LPC-KO} mice. (**E**) Western blot analysis on primary hepatocyte extracts from 6-week-old WT and RIPK1^{LPC-KO} mice. (**F**) Western blot analysis on primary hepatocytes from WT and RIPK1^{LPC-KO} mice treated with TNF for the indicated time points in the absence or presence of the proteasomal inhibitor MG132. NP-40 lysates were prepared and the soluble and insoluble fractions were analyzed. (**G**) Western blot analysis of primary hepatocytes from WT and RIPK1^{LPC-KO} mice treated with TNF for the indicated time points. Necrostatin-1 (Nec1) was added 1 hr prior to TNF stimulation. (**H**) Functionality of Nec1s and Nec1 was confirmed in TNF treated L929 cells after 16 hr. (**I**) Statistical analysis of cell death measured by MTT assay and Western Blot analysis for MLKL phosphorylation to test necroptosis activation after 16 hr. Note that necroptotic cell death in response to TNF was detectable in DMSO and zVAD treated but not in Nec1s and Nec1 treated L929 cells. Results are expressed as mean, +/- SEM. ***p < 0.001 (n = 4). (**J**) PCR analysis of genomic DNA isolated from tails of WT (+/+), heterozygous (+/KD) and homozygous RIPK1 (KD/KD) mice.
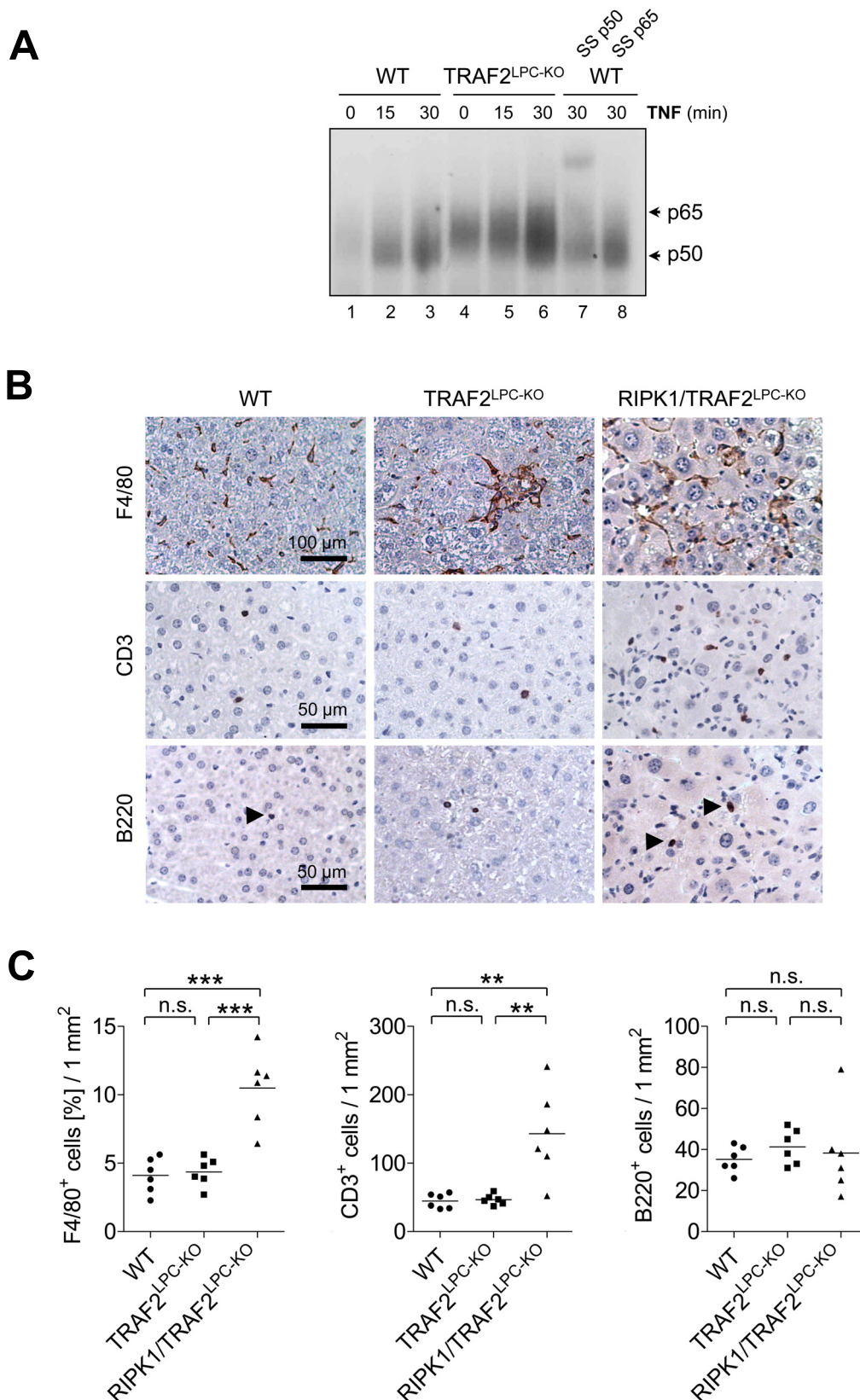
Figure S5, related to Figure 5. RIPK1/TRAF2^{LPC-KO} mice showed increased inflammation compared to WT and TRAF2^{LPC-KO} mice.

(**A**) EMSA on nuclear extracts from primary hepatocytes of WT and TRAF2^{LPC-KO} mice stimulated with TNF for different time points. Antibodies against the NF-κB subunits p50 (lane 7) and p65 (lane 8) were added as supershift controls. (**B**) IHC analysis of F4/80^+, CD3^+ and B220^+ cells on representative liver sections from 6-week-old WT, TRAF2^{LPC-KO} and RIPK1/TRAF2^{LPC-KO} mice. Arrow heads indicate B220^+ cells. (**C**) Statistical analysis of F4/80^+, CD3^+ and B220^+ cells in WT, TRAF2^{LPC-KO} and RIPK1/TRAF2^{LPC-KO} mice. Results are shown as mean. **$p < 0.01$; ***$p < 0.001$; n.s. = not significant ($n = 6$).

A

RIPK1/TRAF2^{LPC-KO}

B

RIPK1/TRAF2^{LPC-KO}

C

WT

RIPK1/TRAF2/
Casp-8^LPC-KO

kDa

50 — TRAF2

80 — RIPK1

60 — Casp-8

30 — GAPDH

1 2 3 4 5 6

D

WT

RIPK1/
TRAF2^LPC-KO

RIPK1/TRAF2^LPC-KO/
RIPK3^-/-

kDa

50 — TRAF2

80 — RIPK1

50 — RIPK3 *

30 — GAPDH

1 2 3 4 5 6 7 8 9

E

WT

RIPK1/
TRAF2^LPC-KO

RIPK1/TRAF2^LPC-KO/
RIPK3^-/-

6 weeks

1 cm

F

ALT [U/l]

GLDH [U/l]

2500
2000
1500
1000
500

**
***   n.s.

4000

3000

2000

1000

**
***   n.s.

● WT   ■ RIPK1/TRAF2^LPC-KO
▲ RIPK1/TRAF2^LPCKO/RIPK3^-/-

G

WT

RIPK1/TRAF2^LPC-KO

RIPK1/TRAF2^LPCKO/
RIPK3^-/-

H/E

200 μm

100 μm

cl. Casp-3

100 μm

KI67

50 μm

H

cl.Casp-3^+ hepatocytes /
1000 hepatocytes

20

15

10

5

0

*
***   n.s.

Ki67^+ hepatocytes /
1000 hepatocytes

500

400

300

200

100

0

***
***   n.s.

● WT   ■ RIPK1/TRAF2^LPC-KO
▲ RIPK1/TRAF2^LPCKO/RIPK3^-/-

I

WT

RIPK1/
TRAF2^LPC-KO

RIPK1/TRAF2^LPC-KO/
RIPK3^-/-

kDa

15 — cl. Casp-3

30 — PCNA

30 — GAPDH

1 2 3 4 5 6 7 8 9

J

WT

RIPK1/TRAF2^LPC-KO

50-52 weeks

1 cm

RIPK1/TRAF2^LPC-KO/RIPK3^-/-

Figure S6, related to Figure 6. Additional deletion of *Ripk3* in RIPK1/TRAF2^{LPC-KO} mice did not prevent HCC development.

(**A**) H/E staining of 52-week-old RIPK1/TRAF2^{LPC-KO} mice revealed tumors of various histopathology including clear cell variants of HCCs. (**B**) Distribution of cl. Caspase-3$^+$ and Ki67$^+$ hepatocytes among tumorous and peritumorous tissue in RIPK1/TRAF2^{LPC-KO} mice. (**C**) Western blot analysis on liver extracts from WT and RIPK1/TRAF2/Caspase-8^{LPC-KO} mice. (**D**) Western blot analysis on liver extracts from WT, RIPK1/TRAF2^{LPC-KO} and RIPK1/TRAF2^{LPC-KO}/RIPK3$^{-/-}$ mice. * = nonspecific band. (**E**) Macroscopic pictures of livers from the indicated 6-week-old mice. Livers of RIPK1/TRAF2^{LPC-KO} and RIPK1/TRAF2^{LPC-KO}/RIPK3$^{-/-}$ mice show multiple small nodules and an icteric color. (**F**) Serum level analysis of ALT and GLDH from 6-week-old mice. Results are shown as mean. **$p < 0.01$; ***$p < 0.001$; n.s. = not significant (n = 6). (**G**) Histologi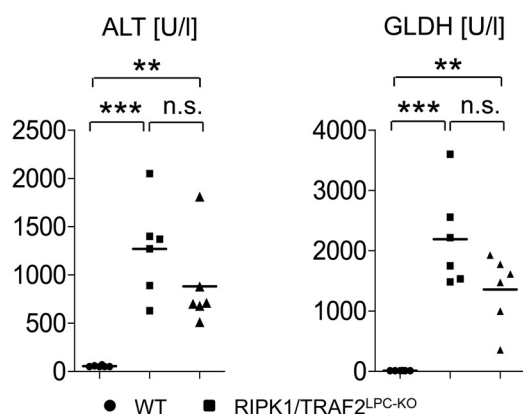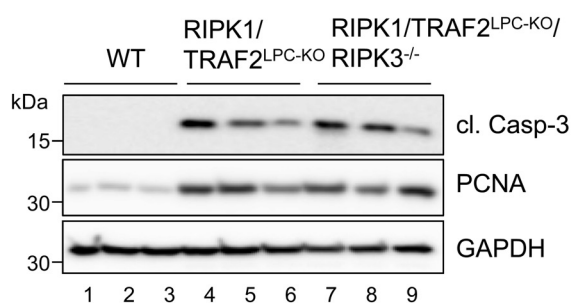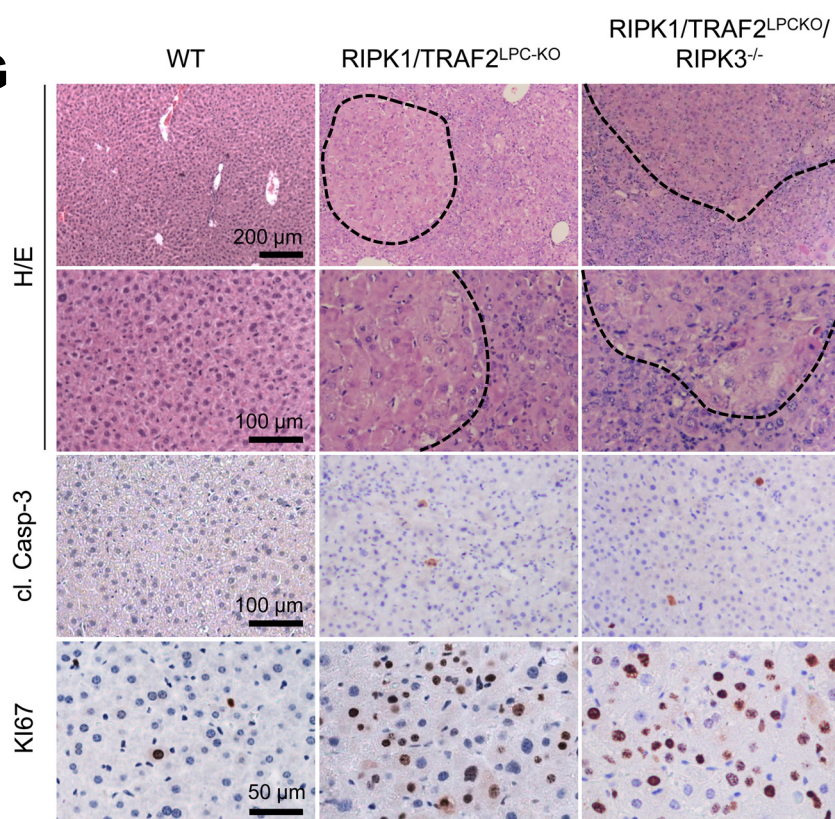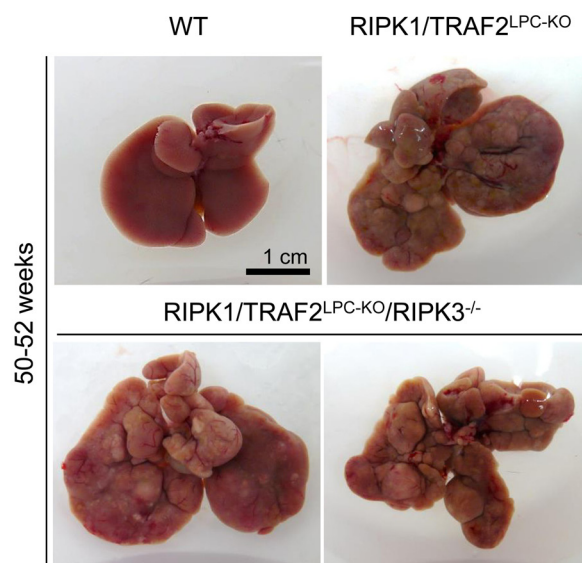cal analysis on liver sections obtained from 6-week-old mice. Areas of hepatocellular dysplasia are indicated by H/E stainings on RIPK1/TRAF2^{LPC-KO} and RIPK1/TRAF2^{LPC-KO}/RIPK3$^{-/-}$ liver sections. IHC staining of cl. Caspase-3$^+$ and Ki67$^+$ cells on liver slides from 6-week-old mice. (**H**) Quantification of cl. Caspase-3$^+$ and Ki67$^+$ hepatocytes of the indicated mice. Results are shown as mean. *$p < 0.05$; ***$p < 0.001$; n.s. = not significant (n = 6). (**I**) Western blot analysis on liver extracts from 6-week-old mice. (**J**) Representative macroscopic pictures of 50-52-week-old mice display multiple large liver tumors in the RIPK1/TRAF2^{LPC-KO} and RIPK1/TRAF2^{LPC-KO}/RIPK3$^{-/-}$ mice.
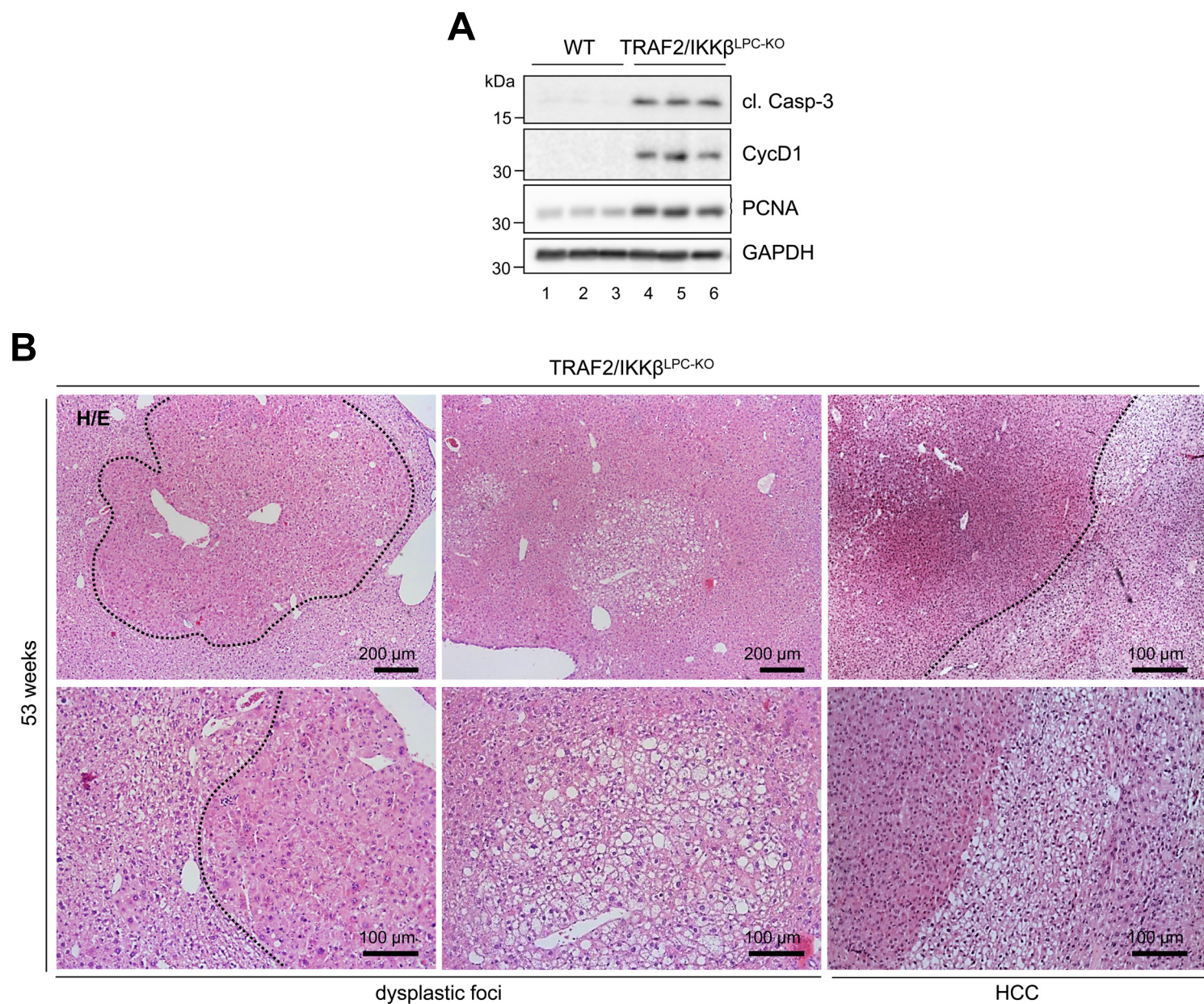
Figure S7, related to Figure 7. TRAF2/IKKβ^{LPC-KO} mice develop adenomatous hyperplasia, dysplastic foci and HCC.
(**A**) Western blot analysis on liver extracts from 6-week-old WT and TRAF2/IKKβ^{LPC-KO} mice. (**B**) H/E staining on liver sections of 53-week-old TRAF2/IKKβ^{LPC-KO} mice revealed adenomatous hyperplasia, dysplastic foci and HCC.

Table S1, related to Figure 6 and 7. Histological quantification of liver tumors.

RIPK1^{LPC-KO} → RIPK1^{LPC-KO}

Nr.	Mouse Nr.	Sex	Age in weeks	Tumor	Grading
1.	267	male	52 w	-	-
2.	480	male	52 w	-	-
3.	486	male	52 w	-	-
4.	713	male	52 w	-	-
5.	54	male	52 w	-	-

TRAF2^{LPC-KO}

Nr.	Mouse Nr.	Sex	Age in weeks	Tumor	Grading
6.	372	male	44 w	-	-
7.	476	male	52 w	-	-
8.	477	male	52 w	-	-
9.	466	male	52 w	-	-
10.	569	male	52 w	-	-

RIPK1/TRAF2^{LPC-KO}

Nr.	Mouse Nr.	Sex	Age in weeks	Tumor	Grading
11.	50	male	50 w	+	HCCs: G2-3
12.	74	male	53 w	+	HCC: G3
13.	114	female	52 w	+	HCCs: G2-3
14.	118	female	52 w	+	HCCs: G2-3
15.	124	female	50 w	+	HCCs: G1-3
16.	139	male	52 w	+	HCCs: G2-3
17.	164	male	52 w	+	HCCs: G2-3
18.	204	male	51 w	+	HCCs: G2-3
19.	205	male	51 w	+	HCCs: G2-3
20.	203	male	58 w	+	HCCs: G2-3

RIPK1/TRAF2/Caspase-8^{LPC-KO}

Nr.	Mouse Nr.	Sex	Age in weeks	Tumor	Grading
21.	168	male	50 w	-	-
22.	174	male	50 w	-	-
23.	197	male	50 w	-	-
24.	201	male	52 w	-	-
25.	208	male	50 w	-	-

TRAF2/IKKβ^{LPC-KO}

Nr.	Mouse Nr.	Sex	Age in weeks	Tumor	Grading
26.	71	female	53 w	+	adenomatous hyperplasia, dysplastic foci
27.	83	male	53 w	+	HCC: G1
28.	98	female	51 w	+	adenomatous hyperplasia, dysplastic foci
29.	99	female	51 w	+	adenomatous hyperplasia, dysplastic foci
30.	102	female	53 w	+	adenomatous hyperplasia, dysplastic foci
31.	107	male	53 w	+	adenomatous hyperplasia, dysplastic foci
32.	144	male	51 w	+	adenomatous hyperplasia, dysplastic foci
33.	165	male	50 w	+	adenomatous hyperplasia, dysplastic foci

Table S2, related to Figure 8. Patients´ characteristics of the HCC tissue microarray (TMA) cohort.

Gender	
male	83 (84%)
female	16 (16%)
Median age (range)	63 (33-81)
Median survival (range)	33 (0-126) months
Etiology	
HBV	9 (9%)
HBV + alcohol	4 (4%)
HCV	15 (15%)
HCV + alcohol	1 (1%)
co-infection	3 (3%)
alcohol	20 (20%)
non-alcoholic fatty liver disease	17 (17%)
cryptogenic	26 (27%)
genetic hemochromatosis	4 (4%)
Grading	
well differentiated HCC	13 (13%)
moderately differentiated HCC	62 (63%)
poorly differentiated HCC	24 (24%)
Tumor size	
< 2.0 cm	3 (3%)
2 .0 – 5.0 cm	45 (45%)
> 5.0 cm	51 (52%)
No. of nodules	
1	69 (70%)
2	10 (10%)
3	3 (3%)
>3	17(17%)
UICC stage	
I	38 (39%)
II	30 (30%)
IIIa	23 (23%)
IIIb	3 (3%)
IIIc	4 (4%)
IV	1 (1%)
Vascular invasion	
present	47 (47%)
none	52 (53%)

SUPPLEMENTAL EXPERIMENTAL PROCEDURES

Tissue microarrays (TMA) and immunohistochemistry of human HCC

A TMA containing 104 HCC samples, derived from liver resections performed at the University Hospital Heidelberg between 2001 and 2010, was constructed as described (Longerich et al., 2004). The median age was 63 years (range 33 to 81) and the male/female ratio was 4:1. All diagnoses were confirmed by histological re-evaluation and use of the samples was approved by the local ethics committee of the University Hospital Heidelberg (approval no: 206/2005). Detailed clinicopathological characteristics are shown in Table S2. Immunohistochemistry (IHC) was performed on 3 μm sections. Antigens of RIPK1 and TRAF2 were retrieved using citrate buffer (pH 6.1, Dako) and detected using the following primary antibodies: anti-human TRAF2 (Abcam, 1:100), anti-human RIPK1 (Novus, 1:750). Counterstaining was performed using Mayer´s hemalum (Merck Millipore). Evaluation of both RIPK1 and TRAF2 was technically possible in 99 patients. Stainings were assessed using the immunoreactive (IR)-score (Remmele and Stegner, 1987).

Hepatocyte isolation

Primary hepatocytes were isolated as previously described (Luedde et al., 2008) and cultured in Dulbecco's modified Eagle's medium (DMEM, PAN Biotech) supplemented with 10% fetal calf serum (FCS, PAN Biotech), penicillin (100 U/ml, PAN Biotech) and streptomycin (0.1 mg/ml, PAN Biotech). After pre-treatment with Nec1s (10 µM, BioVision), Nec1 (10 µM, Santa Cruz) or DMSO as control for 1 hr, the primary hepatocytes were stimulated with recombinant mouse TNF (10 ng/ml, HiSS Diagnostics) for the indicated time points. For proteasomal inhibition primary hepatocytes were pre-treated with Bortezomib (10 µM, ChemieTek), MG132 (50 µM, Selleckchem) or vehicle (DMSO) for 4 hr. Recombinant human Fas Ligand/CD95L (70 ng/ml, Peprotech) and murine TRAIL (200 ng/ml, Peprotech) were used to stimulate primary hepatocytes for the indicated time points.

Serum-Analysis

Serum ALT, AST, GLDH and AP activities were measured by standard procedures in the Institute of Clinical Chemistry of the RWTH University Hospital Aachen.

Plasmids

The expression vectors RIPK1-HA-GFP [plasmid 41396; (Cho et al., 2009)] and 3xMyc-TRAF2 [plasmid 44104; (Shen et al., 2012)] were obtained from Addgene. HA-ubiquitin plasmid was a gift from Gilles Courtois, INSERM U1038, BIG, CEA, Grenoble, France.

Cell Culture and transient transfection

HepG2, Hepa1-6 and L929 (ATCC® CCL-1™) cells were cultured in DMEM supplemented with 10% FCS, penicillin (100 U/ml) and streptomycin (0.1 mg/ml). Transient transfection of Hepa1-6 cells in six-well dishes was carried out using FuGENE HD transfection reagent (Promega) according to the manufacturer's protocol. L929 cells were pretreated by zVAD (20 µM, Merck Millipore), Nec1s (10 µM, BioVision), Nec1 (10 µM, Santa Cruz) or vehicle (DMSO) for 1 hr followed by recombinant mouse TNF (10 ng/ml, HiSS Diagnostics) treatment for 15 hr. MTT cell proliferation assay was performed accordingly to manufacturer's instructions (Thermo Scientific).

Quantitative real-time PCR (qRT-PCR)

Total RNA was purified from primary hepatocytes using Trizol reagent (Invitrogen) and an RNeasy Mini Kit (Qiagen). The quantity and quality of the RNA was determined spectroscopically using a nanodrop (Thermo Scientific). Total RNA (1 µg) was used to synthesize cDNA using the Transcriptor cDNA First-Strand Synthesis Kit (Peqlab) according to the manufacturer's protocol. cDNA samples (2 µl) were used for qRT-PCR in a total volume of 25 µl using SYBR Green Reagent (Invitrogen) and specific primers on a qPCR machine (Applied Biosystems 7300 Sequence Detection System). All qRT-PCR reactions were performed in duplicates. Data were generated and analyzed using SDS 2.3 and RQ

manager 1.2 software. Primer sequences are available upon request. All values were normalized to the level of β-actin mRNA. The expression of *A20* and *IκBα* was tested using the primers as follows: A20: 5'-GAACAGCGATCAGGCCAGG-3' (for), 5'-GGACAGTTGGGTGTCTCACATT-3' (rev); IκBα: 5'-TGAAGGACGAGGAGTACGAGC-3' (for), 5'-TTCGTGGATGATTGCCAAGTG-3' (rev); β-actin: 5′-CTCTAGACTTCGAGCAGGAGA TGG-3′ (for), 5′-ATGCCACAGGATTCCATACCCAAGA-3′ (rev).

Co-Immunoprecipitation (IP)

IP-experiments were performed as previously described (Gautheron et al., 2010). Briefly, Hepa1-6 cells were recovered by gentle pipetting in 1 ml of phosphate-buffered saline (PBS, PAN Biotech). They were centrifuged at 6000 rpm for 1 min in a microfuge and resuspended in 50–100 ml of TNT buffer [20 mM Tris-HCL (pH 7.5), 1% Triton X-100, 200 mM NaCl]. After incubation on ice for 10 min and centrifugation at 14000 rpm for 10 min, the supernatant was recovered and the protein concentration determined. Proteins were either directly analyzed by western blotting or Myc-TRAF2 was immunoprecipitated using a mouse anti-c-Myc tag antibody (Thermo Scientific). In this latter case, extracts were incubated under rotation overnight at 4°C with the antibody. Protein G Sepharose (BioVision) was then added and the mixture incubated for 2 hr at 4°C. Sepharose beads were quickly centrifuged in a microfuge (30 s at 10000 rpm) and washed three times with TNT. After the final wash, the beads were resuspended and heated in buffer A [10 mM KCl, 2 mM MgCl2, 0.1 mM EDTA, 1 mM DTT, 10 mM Hepes (pH 7.8)] and sample loading buffer and electrophoresed through a 8% acrylamide gel. Immunoblots were probed with the following antibodies: anti-RIPK1 (BD Biosciences); anti-TRAF2 (Santa Cruz), anti-HA (Origene).

Precipitation of endogenous RIPK1/TRAF2 complexes

1×10^{7} of HepG2 cells were stimulated with Fc-TNF [10 ml of human Fc-TNF supernatant - produced with an expression vector containing Fc-hTNF-(85-233) - as described previously (Bossen et al., 2006)] for 5 min. Precipitation was performed as described before

(Diessenbacher et al., 2008). Briefly, equal amounts from all cell lysates were used for precipitation as well as for input controls. Endogenous proteins were precipitated by co-incubation of all lysates with 40 µl protein G Agarose (Roche) and slowly rotated over night at 4°C. To show specificity of binding upon TNF stimulation, Fc-TNF was added to the non-stimulated HepG2 lysates. Proteins were separated by further Western blot analysis. Immunoblots were probed with the following antibodies: anti-RIPK1 and anti-TRADD (BD Biosciences), anti-TRAF2 (Santa Cruz), anti-cIAP-1 (kindly provided by John Silke), anti-TNFR1 (Santa Cruz) and anti-β-actin (Sigma-Aldrich).

Western blot analysis

Liver tissue or primary hepatocytes were homogenized in NP-40 lysis buffer [50 mM Tris-HCL (pH 7.5), 150 mM NaCl, 0.5% NP-40 supplemented with PhosSTOP™ phosphatase inhibitor (Roche), cOmplete™ protease inhibitor (Roche), 1 mM Pefablock (Roche) and 1 mM 1,4-Dithiothreitol (DTT, Roth)] using a tissue grind pestle (Kimble/Chase) to obtain protein lysates. To generate soluble and insoluble fractions from hepatocyte lysates, the samples were centrifuged at 14.000 rpm for 10 min at 4°C and the soluble supernatants retained. The insoluble pellets of the hepatocyte samples were washed twice with NP-40 buffer, processed by sonication and centrifuged at 14.000 rpm for 20 min at 4°C respectively. Subsequently the pellets were solubilized in Urea-buffer [7 M Urea, 2 M Thiourea, 4% CHAPS, 40 mM Tris-HCL (pH 8.5), 10 mM DTT], sonicated and boiled 10 min with 2x laemmli sample loading buffer (BIORAD). The different fractions were separated by SDS-polyacrylamide gel electrophoresis (PAGE), transferred to PVDF membrane (Merck Millipore) and analyzed by immunoblotting as previously described (Luedde et al., 2003). Membranes were probed with the following antibodies: anti-cleaved-Caspase-3, anti-cleaved-Caspase-8, anti-p-c-Jun, anti-IκBα, anti-p-JNK, anti-JNK, anti-cIAP-1, anti-K48 (Cell Signaling), anti-FLIP (Dave-2, Adipogen), anti-Caspase-8 (Enzo Life Science), anti-β-actin (SIGMA), anti-RIPK1 (BD), anti-RIPK3 (ProSci), anti-CyclinD1, anti-PCNA (ZYMED), anti-TRAF2 (Santa Cruz), and anti-

GAPDH (AbD Serotec). As secondary antibodies, anti-rabbit-HRP, anti-mouse-HRP (GE Healthcare) and anti-rat-HRP (Santa Cruz) were used.

Electrophoretic mobility shift assay (EMSA)

Gel retardation assays were performed on nuclear extracts as described previously (Luedde et al., 2008). DNA protein complexes were resolved on a 6% polyacrylamide gel. A ^{32}P-labeled oligonucleotide (Hartmann analytic) representing an NF-κB consensus site (5'-CGGGCTGGGGAT TCCCCATCTCGGTAC-3') was used as a probe. For supershifts, high-concentrated antibodies against p50 and p65 (Santa Cruz) were used.

Stainings of mouse tissue

Paraformaldehyde (4%) fixed and paraffin embedded liver tissues were cut in sections (2 μm) and stained with H/E [hemalum (Dako) and eosin (Sigma-Aldrich)] or various primary and secondary antibodies. For IHC staining, tissue sections were deparaffinized with xylene and dehydrated in graded alcohols. Antigen retrieval was performed in EDTA-buffer (10 mM Tris, 1 mM EDTA, 0.05% Tween, pH 9) at 98°C for 30 min or Histo/Zyme (Sigma-Aldrich) for 15 min. The sections were then treated with 3% hydrogen peroxidase (H_2O_2) in water for 10 min to block endogenous peroxidase activity and then reacted with normal goat or horse serum (Vector Laboratories) for 30 min. IHC staining was performed with the following primary antibodies at 4°C overnight: anti-F4/80 (Abcam, 1:300), anti-CD3 (Thermo Scientific, 1:500), anti-B220 (BD Biosciences, 1:250), anti-Ki67 (Thermo Scientific, 1:2000), anti-cleaved Caspase-3 (Cell Signaling, 1:750), anti-Collagen IV (Cedarlane, 1:300), anti-RelA/p65 (Santa Cruz, 1:5000). Sections were then incubated with the secondary antibodies: anti-rabbit IgG HRP, anti-rat IgG HRP (Vector Laboratories) and bound antibodies were visualized with 3-3´-diamonobenzidine (DAB, Thermo Scientific). All sections were counterstained with hemalum. Image acquisition was performed on a Leica DM1000 microscope equipped with a Leica EC3 digital camera.

The TUNEL test was performed using the TUNEL kit from Promega according to the instruction manual. Nuclei were visualized by using mounting medium containing DAPI (Vector Laboratories).

Analysis and quantification of immunohistochemical stainings

Hepatocytes positively stained for cl. Caspase-3, Ki67 or RelA/p65 as well as cells positively stained for B220 (B-cells) and CD3 (T-cells) were quantified numerically using ImageJ$^{®}$ software on whole tissue sections. RelA/p65 stainings are represented in % of positive cells per total cells. B220^{+} and CD3^{+} cells were displayed per 1 mm^{2} tissue area and cl. Caspase-3^{+} and Ki67^{+} hepatocytes were normalized per 1000 hepatocytes. The amount of F4/80^{+} monocytes/macrophages was quantified by calculating the covered area (% / 1 mm^{2} tissue area) using ImageJ$^{®}$ software. Positive cells for cl. Caspase-3, Ki67, B220 or CD3 were examined using a Leica DM1000 microscope and 20x magnification (10 visual fields / stained slide). F4/80 and p65 was examined with 10x magnification (10 visual fields / stained slide).

Supplemental References

Bossen, C., Ingold, K., Tardivel, A., Bodmer, J. L., Gaide, O., Hertig, S., Ambrose, C., Tschopp, J., and Schneider, P. (2006). Interactions of tumor necrosis factor (TNF) and TNF receptor family members in the mouse and human. The Journal of Biological Chemistry *281*, 13964-13971.

Cho, Y. S., Challa, S., Moquin, D., Genga, R., Ray, T. D., Guildford, M., and Chan, F. K. (2009). Phosphorylation-driven assembly of the RIP1-RIP3 complex regulates programmed necrosis and virus-induced inflammation. Cell *137*, 1112-1123.

Diessenbacher, P., Hupe, M., Sprick, M. R., Kerstan, A., Geserick, P., Haas, T. L., Wachter, T., Neumann, M., Walczak, H., Silke, J., and Leverkus, M. (2008). NF-kappaB inhibition reveals differential mechanisms of TNF versus TRAIL-induced apoptosis upstream or at the level of caspase-8 activation independent of cIAP2. J Invest Dermatol *128*, 1134-1147.

Gautheron, J., Pescatore, A., Fusco, F., Esposito, E., Yamaoka, S., Agou, F., Ursini, M. V., and Courtois, G. (2010). Identification of a new NEMO/TRAF6 interface affected in incontinentia pigmenti pathology. Human Molecular Genetics 19, 3138-3149.

Longerich, T., Breuhahn, K., Odenthal, M., Petmecky, K., and Schirmacher, P. (2004). Factors of transforming growth factor beta signalling are co-regulated in human hepatocellular carcinoma. Virchows Arch *445*, 589-596.

Luedde, T., Rodriguez, M. E., Tacke, F., Xiong, Y., Brenner, D. A., and Trautwein, C. (2003). p18(INK4c) collaborates with other CDK-inhibitory proteins in the regenerating liver. Hepatology *37*, 833-841.

Remmele, W., and Stegner, H. E. (1987). [Recommendation for uniform definition of an immunoreactive score (IRS) for immunohistochemical estrogen receptor detection (ER-ICA) in breast cancer tissue]. Pathologe *8*, 138-140.

Shen, R. R., Zhou, A. Y., Kim, E., Lim, E., Habelhah, H., and Hahn, W. C. (2012). IkappaB kinase epsilon phosphorylates TRAF2 to promote mammary epithelial cell transformation. Mol Cell Biol *32*, 4756-4768.